BULLETIN DE L'ASSOCIATION MINÉRALOGIQUE DU CANADA

THE CANADIAN MINERALOGIST

JOURNAL OF THE MINERALOGICAL ASSOCIATION OF CANADA

Volume 43 June 2005 Part 3

*The Canadian Mineralogist*
Vol. 43, pp. 857-881 (2005)

# RELICS OF HIGH-TEMPERATURE CLINOPYROXENE ON THE JOIN Di–CaTs WITH UP TO 72 mol.% $Ca(Al,Fe^{3+})AlSiO_6$ IN THE SKARNS OF CICLOVA AND MAGUREAUA VAŢEI, CARPATHIANS, ROMANIA

MARIE-LOLA PASCAL[§]

*CNRS – Institut des Sciences de la Terre d'Orléans, 1A, rue de la Férollerie, F–45071 Orléans, France*

ILDIKO KATONA

*Equipe Pétrologie, Modélisation des matériaux et Processus, Université Paris 6, 4, Place Jussieu, F–75252 Paris, Cedex 05, France, et Unité de Géologie, Université Catholique de Louvain, 3, Place Louis Pasteur, B–1348 Louvain-la-Neuve, Belgium*

MICHEL FONTEILLES

*Equipe Pétrologie, Modélisation des matériaux et Processus, Université Paris 6, 4, Place Jussieu, F–75252 Paris, Cedex 05, France*

JEAN VERKAEREN

*Unité de Géologie, Université Catholique de Louvain, 3, Place Louis Pasteur, B–1348 Louvain-la-Neuve, Belgium*

## ABSTRACT

In the western Carpathians of Romania, clinopyroxene with a very high content of the Ca-Tschermak (up to 24 wt.% $Al_2O_3$) and esseneite components occurs as veinlets and inclusions, in places associated with kalsilite, in calcite and in wollastonite very close to the marble contacts of two shallow monzodioritic intrusive complexes, Magureaua Vaţei, in the Apuseni Mountains, and Oraviţa–Ciclova, in Banat, both of Upper Cretaceous age. These relics originate from magmatic veinlets, emplaced at an early stage of the magmatic process and later recrystallized at high temperature (>800°C) by a $CO_2$-dominated fluid (stage 1). Such fluid probably resulted from the reaction of calcite with the main intrusive body at the time of its emplacement, a reaction also witnessed by the development of a symplectitic association of anorthite and aluminous pyroxene at the intrusive margins, and by the (exceptional) occurrence of Na-rich melilite. Part of the intrusive boundaries were later invaded by pegmatite-forming liquids or fluids that, upon reaction with calcite, first produced idiomorphic crystals of (Fe,Mg)-rich wollastonite (stage 2), occasionally hosting minerals of stage 1, followed by the development of a fibrous wollastonite – grossular association (stage W) accompanied by an (Al-poor) diopside that progressively became Al-rich (stage P) through further modification of the fluid by reaction with calcite. The later appearance of vesuvianite initiated the large-scale postmagmatic hydrothermal process.

*Keywords*: esseneite, Ca-Tschermak component, skarn, banatite, gehlenite, melilite, microsommite, wollastonite, Carpathian Mountains, Romania.

[§] *Present address*: Equipe Pétrologie, Modélisation des matériaux et Processus, Université Paris 6, 4, Place Jussieu, F–75252 Paris, Cedex 05, France. *E-mail address*: mlp@pmmp.jussieu.fr

## Sommaire

Dans les Carpates occidentales roumaines, des clinopyroxènes exceptionnellement riches en composants esseneïte et Ca-Tschermaks (jusqu'à 24% $Al_2O_3$, poids) se présentent en veinules et en inclusions, avec kalsilite généralement associée, dans la calcite et la wollastonite au voisinage immédiat des contacts calcaires de deux intrusions monzodioritiques, Magureaua Vaţei, aux Monts Apuseni, et Oraviţa–Ciclova, dans le Banat, d'âge tardi-Crétacé. Ces pyroxènes se sont développés à T > 800°C par recristallisation de veinules intrusives, mises en place dans le calcaire à un stade précoce de l'histoire magmatique, sous l'effet d'un fluide à $CO_2$ dominant, probablement produit par réaction de la calcite avec le magma lors de phase principale de mise en place du magma (stade 1). D'autres témoins de cette réaction sont le développement de symplectites à anorthite – pyroxène alumineux dans les bords de l'intrusion, ainsi qu'une exceptionnelle présence de mélilite sodique. Les contacts intrusifs ont ensuite été partiellement envahis par des liquides ou fluides « pegmatitiques » (stade 2) qui, toujours par réaction avec la calcite, ont d'abord précipité des cristaux idiomorphes de wollastonite riche en (Fe,Mg), piégeant parfois des minéraux du stade 1, puis développé une association wollastonite fibreuse – grossulaire accompagnée d'un diopside devenant alumineux à mesure que la composition du fluide se modifiait par réaction avec la calcite. Puis l'apparition de vésuvianite marque le début des processus hydrothermaux postmagmatiques à grande échelle.


*Mots-clés*: esseneïte, composant Ca-Tschermak, skarn, banatite, gehlenite, mélilite, microsommite, wollastonite, Carpates, Roumanie.

## Introduction

Clinopyroxenes enriched in the CaTs ($CaAl_2SiO_6$) component reflect conditions of formation under either very high pressure, such as found in eclogite inclusions in kimberlite or in nephelinite pipes (Lovering & White 1969, Bobrievich *et al*. 1959, in Deer *et al*. 1978), or strong silica-undersaturation such as found in alkaline rocks including carbonatites (Peacor 1967, Huckenholz 1973, Cundari 1982) and in pyrometamorphism of calcareous rocks (and the resultant associated skarns). In the latter case, such pyroxene is commonly also enriched in the esseneite ($CaFe^{3+}AlSiO_6$) and Ca–Ti-Tschermak ($CaTiAl_2O_6$) components. Such Al-rich, Ti-rich and Si-poor pyroxenes also occur in meteorites (Dodd 1971, Hazen & Finger 1977, Blander & Fuchs 1975).

The processes involved in the formation of peraluminous pyroxene in skarns and their bearing on the subsequent skarn-forming processes are the focus of the present study, in which we report finding, in three occurrences of high-temperature skarns from the Carpathian Mountains in Romania, pyroxene crystals with a range of Al contents reaching values higher than ever reported in literature. Two compositions of one crystal plot in the CaTs field in a plot in terms of $Ca(Mg,Fe^{2+},Mn)Si_2O_6$–$CaAlAlSiO_6$–$CaFe^{3+}AlSiO_6$, *i.e*., corresponding to a new mineral species; unfortunately, the crystal is too small to be extracted for a formal description of its properties, and is here provisionally referred to as "ferrian CaTs".

## Al- and $Fe^{3+}$-Rich Clinopyroxenes and Their Occurrences

Experimental work (Hijikata 1968, Hijikata & Onuma 1969, Onuma *et al*. 1981, Gasparik 1984) and natural occurrences suggest that there is complete solid-solution among pyroxenes in the system $CaMgSi_2O_6$–$CaAl_2SiO_6$–$CaFeAlSiO_6$ (Cosca & Peacor 1987). However, no naturally occurring pyroxene has yet been reported to have a composition in the field "CaTs" (Fig. 1), in contrast with the existence of natural esseneite. For instance, esseneite with up to 80 mol% of the Ess end-member was reported and defined as a new mineral (Cosca & Peacor 1987) from paralavas produced by natural combustion of coal in Wyoming (Cosca & Peacor 1987, Foit *et al*. 1987). Accompanying minerals include melilite, anorthite and iron oxides. The same origin was proposed for the assemblage of very high-temperature calc-silicates of the Mottled Formation in Israel, which contains esseneite with 50% Ess and 15% CaTs (Gross 1977), and for rocks containing the assemblage melilite – wollastonite – anorthite – Ti-rich clinopyroxene (–glass) rocks from Colle Fabri, central Apennines, Italy (Melluso *et al*. 2003).

Clinopyroxene enriched in Al, $Fe^{3+}$ and Ti is commonly reported in high-temperature skarns and calcareous rocks affected by high-grade contact-metamorphism, such as found at contacts of basaltic flows (Havette *et al*. 1982) and dykes (Tilley & Harwood 1931, Sabine 1975), and in metasedimentary material included in mafic intrusions (*e.g*., xenoliths with Al- and Ti-rich clinopyroxene associated with monticellite, spinel and either forsterite or åkermanite in the Kiglapait intrusion, Owens 2000). Some skarn ejecta found at Italian volcanos (Monte Somma – Vesuvius, Vulsini) contain Al-rich pyroxene (Hermes & Cornell 1981, 1983, Varekamp 1983), as does a rock containing the assemblage kaliophilite – pyroxene – melilite – calcite (Scacchi 1888, quoted in Dana 1915). A nodule containing Al-rich pyroxene associated with wollastonite, anorthite and grossular was found at Saint Vincent, Lesser Antilles (Arculus & Wills 1980). Similar associations containing melilite and Al-rich pyroxene are found in metamorphosed limestones and skarns developed at the boundaries of calc-alkaline intrusions. Examples involve, among others, the quartz

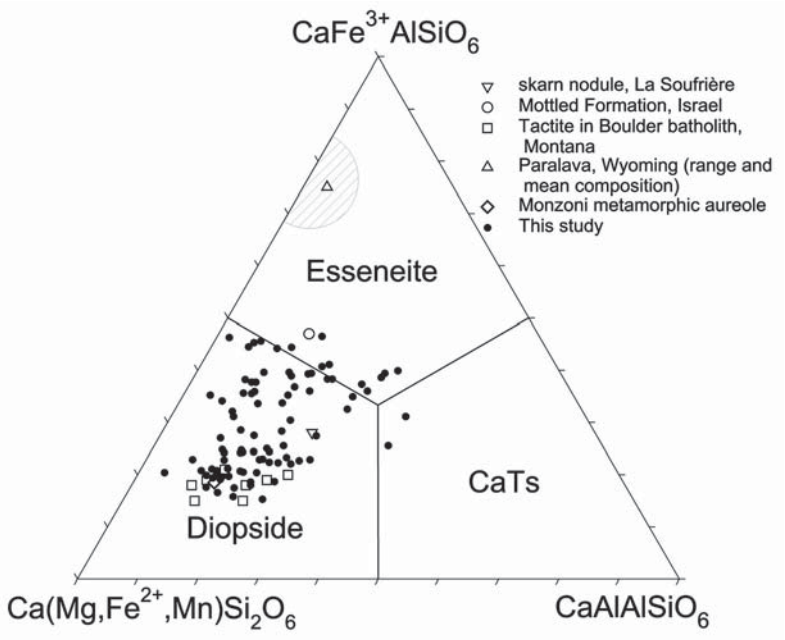


FIG. 1. Representative compositions of natural pyroxene projected in the system $Ca(Mg,Fe^{2+},Mn)Si_2O_6$–$CaAlAlSiO_6$–$CaFe^{3+}AlSiO_6$. This projection (Cosca & Peacor 1987) shows the fields corresponding to dominant $Fe^{3+}$ (esseneite) and Al (CaTs) in the *M*1 site. Data from Gross (1977), Shedlock & Essene (1979), Arculus & Wills (1980), Peacor & Cosca (1987), Foit *et al.* (1987), Povoden *et al.* (2002).

monzonite porphyry at Crestmore, California (Burnham 1959, Wiechmann 1995), monzonites and monzodiorites at Kushiro, Japan (Numano 1978, 1979), at Monzoni, Italy (Tilley 1938, Povoden *et al.* 2002), and at the Apuseni Mountains, Romania (Pascal *et al.* 2001). Septa with Al-rich pyroxene, spinel, garnet, clintonite and vesuvianite occur in a mafic part of the Boulder Batholith, Montana (Shedlock & Essene 1979), and an association of melilite, Al-rich clinopyroxene, kalsilite, phlogopite, wollastonite and calcite was reported by Jamtveit *et al.* (1997) from what may have been a roof pendant near the border of a large intrusive body of larvikite related to the Oslo rift.

The conditions of formation of such rocks are estimated to be at least about 800°C and, in the case of assemblages containing melilite and associated calcium silicates such as wollastonite or, less commonly, spurrite, tilleyite, rankinite or larnite, a low pressure of $CO_2$ (*e.g.*, Reverdatto *et al.* 1979, Wiechmann 1995, Jamtveit *et al.* 1997, Pascal *et al.* 2001, Povoden *et al.* 2002). Such a high temperature strongly suggests that at least in the cases of the intrusions of silicic magma cited above, the processes involved in the formation of these rocks cannot be entirely interpreted as the result of infiltration metasomatism produced in limestones by a *postmagmatic* fluid, as assumed in the classical models for skarn formation. Another feature of these "skarns" that casts a doubt on their relevance to the metasomatic model is the evidence for Al transfer involved in the development of the high-temperature silicate associations from relatively pure magnesian limestones (Crestmore: Burnham 1959), and also for Mg (and Ti) transfer in the case of pure calcitic marbles (occurrences in the Apuseni Mountains: Pascal *et al.* 2001, this study). In addition, the $CO_2$-poor conditions mentioned above cannot account for the presence of Al-rich, Si-poor pyroxene, especially where associated with calcite (Pascal *et al.* 2001). An apparent lack of equilibrium between the Al-rich pyroxene and wollastonite has also been emphasized by Arculus & Wills (1980).

## THE GEOLOGICAL CONTEXT

The skarns in which the ferrian CaTs pyroxene was found are remarkable by the occurrence of rocks mainly composed of gehlenite-rich melilite in bands a few meters or tens of meters long, developed along the contacts between limestones and intrusive bodies that belong to the "banatitic" belt. The Late Cretaceous to Paleocene "banatitic" magmatic-metallogenetic belt (BMMB, Berza *et al.* 1998) extends from western Romania (Apuseni Mountains and Banat) to the Black

Sea through the Timok area in Serbia and Srednogorie zone in Bulgaria (Fig. 2). It includes calc-alkaline high-level plutonic suites and some subordinate volcanic sequences. In respect to their country rocks and geodynamic setting, the magmatism corresponds to post-orogenic processes immediately following the Laramian stage of folding in the Carpathian Mountains, and is interpreted to represent either post-collisional or Andean-type processes (Neubauer 2002). Associated cases of mineralization include major porphyry Cu, massive sulfide deposits, epithermal deposits, hydrothermal veins and skarns (Berza *et al*. 1998).

In spite of their large variability both in structure and quantitative mineralogical composition, these rocks, including granites, syenites, and diorites, porphyritic or not, share a K- and Mg-rich character (Codarcea 1932). A recent synthesis of geochemical data confirms their relatively homogeneous signature, dominantly granodioritic, with medium-K and high-K types (Dupont *et al*. 2002). A few complexes include relatively mafic members of the association, *e.g*., gabbrodiorite, monzogabbro, diorite and monzodiorite, belonging to the high-K type and interpreted to have been emplaced at an early stage of magmatic activity (Russo-Sandulescu & Berza 1979). Such is the case of the Magureaua Vaței and Oravița–Ciclova complexes, in which both gehlenite-rich rocks and Al-rich pyroxene were found.

The *Magureaua Vaței* monzodiorite is located in the Apuseni Mountains (northwestern Romania, Fig. 2), near Vața Bai. It outcrops as several bodies, perhaps belonging to a single larger mass, intruded in Neojurassic calcitic limestones. The *Oravița–Ciclova* intrusive complex crops out between the town of Oravi□a (north) and the valley of the Ciclova (south), in the Banat region (southwestern Romania) (Fig. 2). Whereas gabbrodiorite and diorite have been found in the area of Oravița, the southernmost part of the complex is dominantly monzodioritic to monzonitic. The surrounding terranes in the study area belong to the Getic nappe, emplaced during the Laramian stage of folding and composed of Upper Jurassic limestones (containing dolomite layers) and Cretaceous calcitic limestones and marls.

## The Main Features of the Skarns and Gehlenite-Bearing Rocks

### *The Magureaua Vaței complex*

At Magureaua Vaței, the (barren) skarns are restricted to two small outcrops of gehlenite-bearing rocks, at Cornet Hill and at Upper Cerboaia Valley (Fig. 2), first reported by Ştefan *et al*. (1978) and recently studied in more detail by Pascal *et al*. (2001) and Marincea *et al*. (2001). In both skarn outcrops mentioned, gehlenite ($Gh_{\sim 60}$) + some Ti-rich garnet (Ti up to 0.58 atoms per formula unit, *apfu*) occurs as centimetric to metric veins, mainly at the exoskarn–endoskarn boundary or close to it in the exoskarn. The endoskarn shows an overall zonation, from a gehlenite–wollastonite zone, followed by a grossular – fibrous wollastonite (+ minor diopside) zone on the side of the intrusive rock. The exoskarn consists of spurrite – tilleyite – wollastonite at Cornet Hill, and wollastonite – calcite – Ti-rich garnet in the Upper Cerboaia Valley. The gehlenite-rich band is irregular in thickness and even discontinuous, so that in a few samples, the grossular – fibrous wollastonite endoskarn is observed in direct contact with the coarse wollastonite–calcite exoskarn (except for the very local development of Ti-rich garnet along the boundary). The high-temperature gehlenite stage ended with the crystallization of volatile (fluorine, sulfur, phosphorus)-rich minerals ("ellestadite", cuspidine), suggesting a magmatic origin for the fluid. (The "ellestadite" is in fact a hydroxyl-dominant phase intermediate between ellestadite and apatite groups). Vesuvianite appears in comparatively small amounts as a product of alteration of gehlenite in exoskarns and as a later-formed mineral associated with serpentine in the wollastonite–grossular endoskarn.

### *The Oravița–Ciclova complex*

At Oravița–Ciclova, a skarn cap is preserved at many places over the intrusion. Apart from the sporadic occurrence of very dark skarn rocks mainly composed of well-crystallized late-stage andradite associated with Cu, W and Bi mineralization, most of the skarns are barren, with an striking predominance of yellow vesuvianite on the inner (intrusion) side and some coarse-grained wollastonite on the outer (metamorphosed limestone) side. This vesuvianite-dominated zonation corresponds to the most extensive of the later stages of development of the barren skarns. Where the limestone is not magnesian, the vesuvianite postdated a stage characterized by an extensive development of grossular associated with diopside. In contrast, coarse clintonite, some monticellite and some Al-bearing clinopyroxene occur at the intrusive contact with magnesian marble, which crops out in the Ciclova Valley (Katona 2004).

The most conspicuous exception to the general scheme just described is a small occurrence (15 m in diameter at most) of rocks mainly composed of gehlenite-rich melilite ($Gh_{45–55}$) in the Crişenilor ravine (Fig. 2), reported by Constantinescu *et al*. (1988) and Ilinca *et al*. (1993), and recently studied by Katona *et al*. (2003) and Katona (2004). On every side and even at places inside this area, the gehlenite rocks are altered to the vesuvianite paragenesis. The gehlenite rocks have been interpreted as corresponding to an early, high-temperature stage similar to that observed at Magureaua Vaței.

## THE CLINOPYROXENE OF UNUSUAL COMPOSITION

Clinopyroxene with extremely high Al and $Fe^{3+}$ contents occur as relics of a still earlier stage. Three modes of occurrence, described in more detail below, have been recognized.

### *Occurrence in endoskarns of a peculiar, wollastonite-free type*

An insight into the mode of formation of Al-rich pyroxene is afforded by the observation, in a few specimens, of clinopyroxene with $^{IV}Al$ up to 0.45 *apfu*, occurring in association with anorthite as a modification of the plagioclase–augite association of the diorite at its margin. The example described, in sample VT41, displays a boundary between a normal, unmodified diorite and its wollastonite-free (and calcite-free) endoskarn counterpart, developed (or preserved) on a thickness of 3 cm. On the other side of the sample, the endoskarn is bounded by an irregular development of the garnet rock (isotropic and anisotropic types of granditic garnet with different Ti contents, zeolites, calcite and diopside) usually observed in the vesuvianite-free parts of the Oravița–Ciclova skarns, in which remnants of the earlier paragenesis of Al-rich pyroxene and anorthite are still preserved.

### *Occurrence as veinlets and inclusions in the marble*

This mode of occurrence is found in the Upper Cerboaia Valley (Magureaua Vaței complex). One example found in the outcrop of gehlenite skarn was already described (sample UCV4–1, Pascal *et al*. 2001) was already described, and found in the outcrop of gehlenite skarn. Such veinlets occur very close to the intrusive contact, and contain clinopyroxene with $^{IV}Al$ in the range 0.21–0.55 *apfu*, $Fe^{3+}$ reaching 0.28 *apfu*, calculated on the basis of a total of four cations. The other example (UCV51, this study) belongs to a small isolated outcrop of marble located in Cerboaia Valley, 300 m downstream from the main outcrop of gehlenite rock. This outcrop shows a contact between brecciated marble containing clinopyroxene with the same mode of occurrence and compositional range as in UCV4–1, and a silicate rock mainly composed of zeolites and containing numerous rounded inclusions of calcite a few mm in diameter, perhaps a former vesiculated igneous rock. Short veins of the silicate rock, cm to mm across, penetrate the marble.

### *Occurrence as very small inclusions scattered in coarse-grained wollastonite in wollastonite–grossular endoskarns*

One example of this mode of occurrence is sample UCVZ (Pascal *et al*. 2001), located close to the sample of marble UCV4–1 and to the gehlenite-rich skarns. The additional examples described in the present study include one specimen (CHX) from the outcrop of gehlenite-rich skarn of Cornet Hill (Magureaua Vaței complex), and three samples (VT54–55–56) collected from a large outcrop, mainly of intrusive material, surrounded by the massive vesuvianite skarns at the entrance of the Țiganilor valley near the Ciclova valley (Oravița–Ciclova complex, Fig. 2). Two of the specimens described (VT54 and 56) contain a former contact between marble (now exoskarn) and diorite (now endoskarn), and one (VT55) contains the contact of the endoskarn with the untransformed diorite. There is a striking similarity between these rocks and the endoskarn sample CHX. The compositional range of the pyroxene is 0.30 to 0.58 *apfu* $^{IV}Al$ *apfu* in UCVZ, 0.40 to 0.63 *apfu* in VT54–55–56 and 0.30 to 0.72 in CHX. The absence of Al-poor compositions is as remarkable as the upper limit.

## MINERALOGY

### *Analytical techniques*

The descriptions that follow are based on detailed observations under the polarizing microscope coupled with extensive analyses of the minerals, performed using electron microprobes (Cameca Camebax, SX50 and SX100) and a JEOL 840 scanning electron microscope equipped with an energy-dispersion spectrometer (EDS). The analytical conditions with both electron microprobes were 15 kV acceleration voltage and a beam current of 40 nA (10 nA for light-element-bearing minerals). The standards include natural minerals (albite, orthoclase, andradite, diopside, fluorite) and synthetic oxides. Data reduction was achieved using a "PAP" correction procedure (Pouchou & Pichoir 1985).

### *Stage 1 in (wollastonite-free) endoskarns: Al- and Fe-rich clinopyroxene + anorthite*

The diorite in sample VT41 is composed of small elongate crystals of plagioclase showing a growth zonation ($An_{60–40}$), clinopyroxene (*mg#* 70, 0.5–3 wt.% $Al_2O_3$, 0.3–0.5 wt.% $Na_2O$) as pale yellow or greenish euhedral crystals with a growth zonation and a core rich in inclusions, and large crystals of green actinolite that are observed side by side with the clinopyroxene at a fraction of millimeter from the endoskarn front. The front is sharp, although in places the magmatic texture can be easily recognized over a few millimeters at the onset of the skarn zone. The first change that occurs is the appearance of a fine-grained symplectite prolonging the plagioclase crystals of the diorite, consisting of calcic plagioclase ($An_{80–100}$) and colorless diopside (in vermicules or, in places, rods) (Fig. 3). The clinopyroxene crystals of the diorite are preserved without visible change, whereas amphibole disappears. The

grain size of the minerals in the symplectite progressively increases, from 5 to 10 μm, then the grain size of the anorthite, still containing granules of pyroxene (Table 1, #43/17), increases, and the grains tend to develop a square shape. The smaller crystals of clinopyroxene have the same grain-size as the anorthite, whereas the larger ones (inherited from the magmatic rock) remain almost unchanged, except for the presence of a more aluminous narrow rim that has the same compositional range as the fine-grained pyroxene (4–9 wt% $Al_2O_3$, Table 1, #43/19). A K-bearing mineral (K-feldspar or, more probably, biotite) was detected by means of electron-microprobe analysis, but did not appear in SEM images and could not be identified under the microscope.

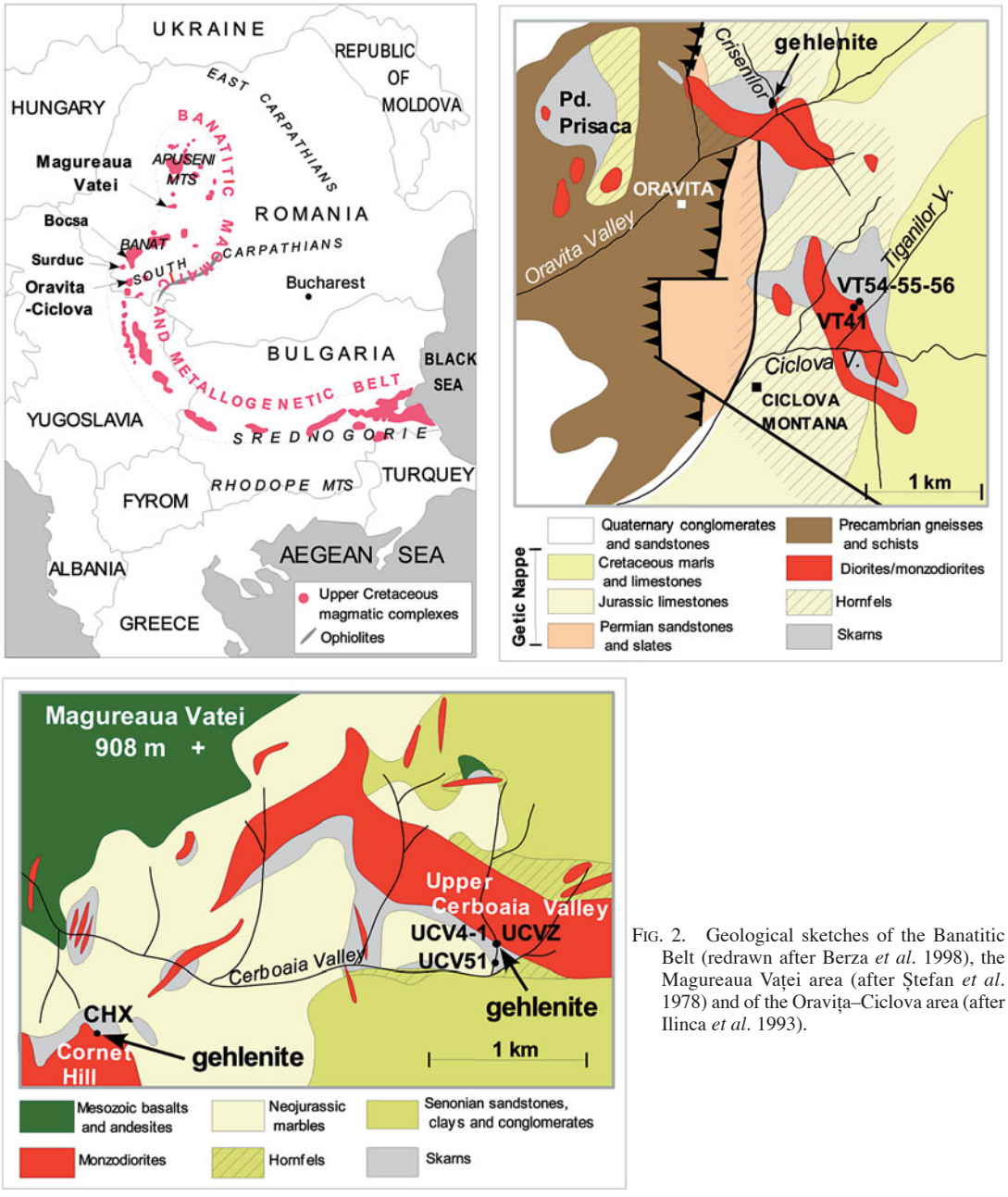


FIG. 2. Geological sketches of the Banatitic Belt (redrawn after Berza *et al.* 1998), the Magureaua Vaței area (after Ștefan *et al.* 1978) and of the Oravița–Ciclova area (after Ilinca *et al.* 1993).

TABLE 1. SELECTED COMPOSITIONS* OF PYROXENE IN ENDOSKARN VT41 (STAGE 1)

| | # | $SiO_2$ | $TiO_2$ | $Al_2O_3$ | FeO | MnO | MgO | CaO | $Na_2O$ | Total | Structural formula | Di | Hd+Jo | Ae | Ess | CaTs | CaTi |
|---|---|---|---|---|---|---|---|---|---|---|---|---|---|---|---|---|---|
| Magmatic clinopyroxene | *43/13* | 53.03 | 0.31 | 1.32 | 6.98 | 0.42 | 14.41 | 24.30 | 0.28 | 101.09 | $Ca_{0.95}Na_{0.02}(Mg_{0.79}Fe^{2+}_{0.15}Mn_{0.01}Ti_{0.01}Fe^{3+}_{0.06})(Al_{0.06}Si_{1.94})O_6$ | 73 | 17 | 2 | 4 | 0 | 1 |
| Symplectite with anorthite | *43/17* | 47.52 | 0.63 | 6.73 | 8.55 | 0.08 | 11.49 | 24.96 | 0.09 | 100.07 | $Ca(Mg_{0.64}Fe^{2+}_{0.13}Ti_{0.02}Al_{0.07}Fe^{3+}_{0.13})(Al_{0.23}Si_{1.77})O_6$ | 64 | 13 | 1 | 13 | 7 | 2 |
| Zoned clino-pyroxene core | *43/21* | 51.50 | 0.68 | 2.15 | 6.15 | 0.20 | 14.39 | 24.36 | 0.31 | 99.74 | $Ca_{0.97}Na_{0.02}(Mg_{0.78}Fe^{2+}_{0.11}Ti_{0.02}Fe^{3+}_{0.08})(Al_{0.09}Si_{1.91})O_6$ | 80 | 11 | 2 | 6 | 0 | 2 |
| rim | *43/19* | 44.22 | 0.77 | 8.60 | 9.50 | 0.17 | 10.43 | 25.00 | 0.03 | 98.72 | $Ca_{1.02}(Mg_{0.59}Fe^{2+}_{0.08}Ti_{0.02}Al_{0.06}Fe^{3+}_{0.22})(Al_{0.32}Si_{1.68})O_6$ | 59 | 9 | 0 | 22 | 6 | 2 |
| Zone of only cpx | *46/35* | 42.26 | 1.09 | 13.48 | 8.10 | 0.10 | 9.53 | 24.74 | 0.02 | 99.69 | $Ca(Mg_{0.54}Fe^{2+}_{0.08}Ti_{0.03}Al_{0.18}Fe^{3+}_{0.17})(Al_{0.42}Si_{1.58})O_6$ | 54 | 8 | 0 | 17 | 18 | 3 |

* established by electron-microprobe analysis. Symbols: Di diopside, Hd: hedenbergite, Jo: johannsenite, Ae: aegirine, Ess: esseneite, CaTs: Ca-Tschermak component, CaTi: Ca–Ti-Tschermak component.

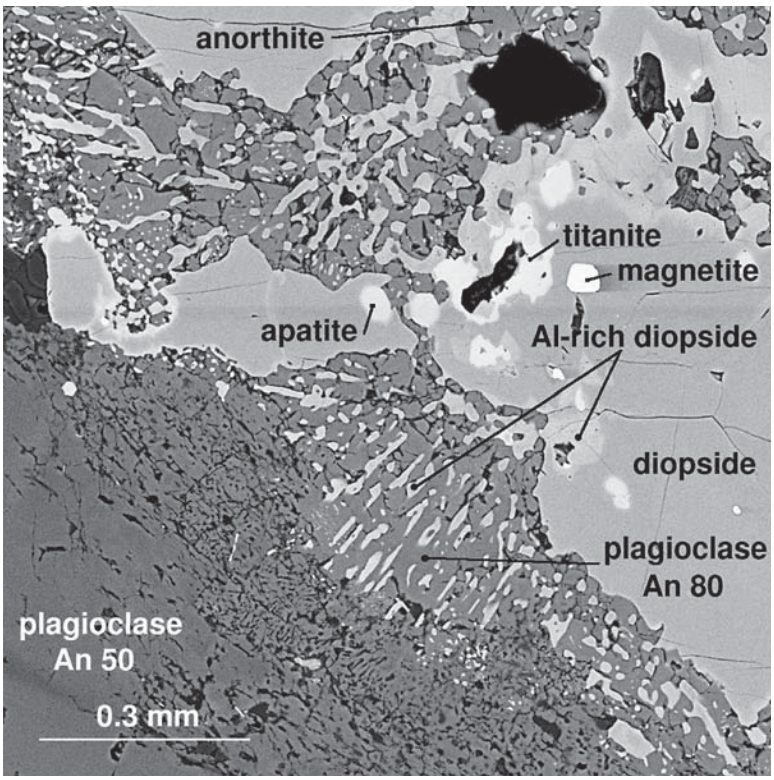


FIG. 3. Stage 1 in the endoskarn VT41. BSE image of the front of endoskarn formation: development of symplectitic intergrowths of calcic plagioclase and Al-bearing pyroxene at the expense of the normal magmatic labradorite of the diorite, followed by an Al-rich pyroxene – anorthite zone. Al-rich zones in pyroxene are lighter-colored.

In the outer part of this zone, the contrast between the two types of pyroxene decreases. The larger crystals lose their original shapes and compositions, still keeping some more-or-less blurred zonations. Then the amount of anorthite strongly but progressively decreases, so that a narrow discontinuous zone made of pyroxene alone can be observed, in which the pyroxene crystals are usually zoned. An irregular periphery with higher Al contents (up to 13 wt.% $Al_2O_3$, Table 1, #46/35), distinctly richer in Al than in the anorthite–pyroxene zone. Anorthite is again present in the outermost zone of the altered skarns.

*Stage 1 in marbles: Al- and Fe-rich clinopyroxene* (±*kalsilite, melilite, microsommite*)

The marble sample UCV4–1 is composed of large crystals of calcite cross-cut by a dense network of silicate veins containing the Al- and Fe-rich clinopyroxene crystals, associated with granditic garnet, especially in the center of comparatively coarse veinlets, and at places with some green spinel. In the calcite-dominant part of the specimen, these veins degenerate into strings of pyroxene granules at the boundaries of calcite crystals, associated with sparse phlogopite and still rarer colorless spinel. The marble is intensely recrystallized with migration of the crystal boundaries, the former location of which is shown by the pyroxene granules.

In the brecciated sample UCV51, the marble fragments are infiltrated by a network of thin veinlets of Al- and Fe-rich pyroxene (Fig. 4a), grading into strings of isolated crystals, resembling those described in UCV4–1. The calcite crystals enclose scarce small (10 μm) grains of silicate minerals (Fig. 4b, Table 2). A few millimeters from the adjacent silicate rock and veins, they include a slightly greenish clinopyroxene, still richer in Al than in the veins, in a few places in contact with kalsilite (or kaliophilite ?), idiomorphic crystals of phlogopite occurring in the immediate vicinity, and occasional idiomorphic microsommite (a K-bearing member of the cancrinite group). Within one millimeter of the silicate rock, Mg- and Na-rich melilite is the only type of silicate included in calcite. The compositional range of the pyroxene, both as inclusions in calcite and in veinlets, is 0.29 to 0.51 *apfu* $^{IV}Al$, with $Fe^{3+}$ up to 0.26 *apfu*, the same as in the veinlets of UCV4–1 (Figs. 5a, b), with variable Ti (up to 0.09 *apfu*, *i.e.*, 3 wt% $TiO_2$), and appreciable Cr (up to 0.26 wt% $Cr_2O_3$). A later-stage association of minerals in the veinlets of UCV51 includes sparse patches of thomsonite, and minor grandite garnet, which tends to occur as a narrow rim between the pyroxene crystals and between thomsonite and calcite (Fig. 4a).

The silicate rock in UCV51 is made of thomsonite with very subordinate diopside and phlogopite in the main body, which also contains rounded patches of inclusion-free calcite, whereas the veins are comprised of a fine-grained association of diopside, grandite garnet and subordinate thomsonite. Along the boundary between calcite and silicates, a thin rim of "skarn" is composed of garnet, thomsonite, muscovite, K-feldspar, and square pseudomorphs (after ?) consisting of a fibrous association of pyroxene and a K-bearing mineral.

The origin of such a rock is not clear, but it allows us to define a stage at which calcite coexisted with Al- and Fe-rich pyroxene and K-bearing minerals (kalsilite and microsommite). Compared to the usual absence of Na from endoskarns at Magureaua Vaţei, the presence of Na-rich silicate minerals in sample UCV51 is another indication that this rock was not modified by the usual endoskarn-forming fluids.

*Relics of stage 1 in wollastonite–grossular endoskarns* (*CHX, VT54–55–56*): *inclusions of Al- and Fe-rich clinopyroxene ± kalsilite*

A few specimens of wollastonite–grossular endoskarns (CHX, VT54–55–56) contain relics of a similar association of minerals. In samples VT54 and VT56, the former marble, now exoskarn composed of wollastonite, calcite and vesuvianite, is clearly identified through the typical morphology of wollastonite crystals, *i.e.*, medium-grained, idiomorphic stout prisms almost devoid of inclusions, and through their idiomorphic relation with the interstitial coarse-grained calcite. The contact between exoskarn and endoskarn is sharp and can be traced in thin section to within about 0.1 mm, in spite of minor irregularities (mainly corresponding to the late development of vesuvianite). The endoskarn, about 10 cm thick, shows a fibrous wollastonite – grossular association in subparallel fibers, organized in a succession of layers parallel to the exoskarn–endoskarn contact and separated by surfaces perpendicular to the fibers (Fig. 6a). This kind of texture is typical of the wollastonite–grossular endoskarn invariably observed in contact with the gehlenite–wollastonite endoskarns. The peculiarity of the samples of interest here is that they contain porphyroblasts of wollastonite (wollastonite *a*, described in the following section and shown in Fig. 6a) that host in their centers small rounded inclusions of green Al- and Fe-rich pyroxene, in some cases associated with kalsilite. Two tiny idiomorphic crystals of biotite were observed included within one such pyroxene + kalsilite inclusion (Fig. 6b).

The compositional range of the pyroxene (the highest Al content was found in CHX, #62/64, Table 2) is similar to that in the samples of marble UCV51 and UCV4–1 for Al, but extends toward higher contents of Fe (both $Fe^{2+}$ and $Fe^{3+}$: Fig 5). No specific correlation is observed among Al and Fe (and Ti, Na, Cr) contents, suggesting that in most cases the Fe (and Ti, Na, Cr) content was not controlled by coexisting phases (fluid or minerals), but was inherited from the pre-existing mineral(s). Compared to the Al-rich pyroxene of VT41, these inclusions of Al- and Fe-rich pyroxene

have higher $^{IV}$Al contents, but part of them plot on the same trend (Fig. 5a), in accordance with the idea that they may represent a further step in the development of the Al-rich pyroxene at the expense of the augite + plagioclase association of the diorite. In contrast, a group of crystals, including those crystals associated with kalsilite, depart from the trend and show higher (and variable) Fe contents. Taking into account the fact that biotite is observed as the product of transformation of the kalsilite–pyroxene association (Fig. 6b), such Fe-rich pyroxene may result from the transformation of biotite.

*Stage 2: Porphyroblasts of wollastonite a in wollastonite–grossular endoskarns* (*CHX, VT54–55–56*)

The samples in which the inclusions described above were found show a complex succession of stages of (incomplete) transformation, in addition to stage 1, including stage 2 characterized by the wollastonite *a* porphyroblasts (Fig. 6a), of interest here, and a series of recrystallization steps responsible for the present state of the groundmass (striped fibrous wollastonite – grossular association cross-cut by various kinds of veins), described in the following section.

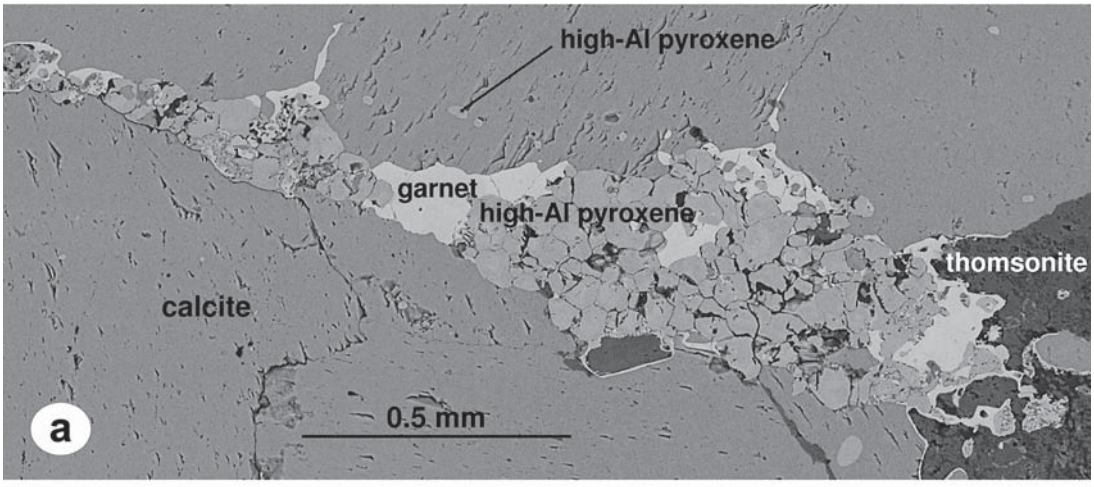


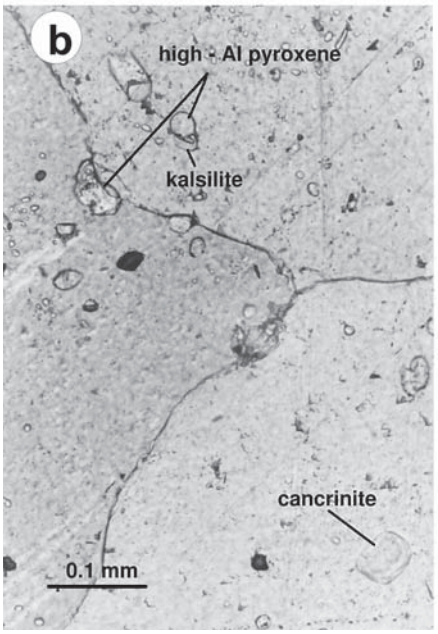


FIG. 4. Stage 1 in the marble UCV51. (a) BSE image of a silicate vein connected with the main silicate rock (lower right) and penetrating into the marble. Inclusions of melilite and pyroxene occur in the neighboring calcite. (b) Photomicrograph of inclusions of kalsilite, pyroxene and microsommite in calcite a few millimeters further from the end of the veinlet shown in (a).

TABLE 2. SELECTED COMPOSITIONS* OF MINERALS OF STAGE 1 INCLUDED IN CALCITE (MARBLE UCV51) OR WOLLASTONITE *a* (ENDOSKARNS CHX, VT55)

| | Sample, # | $SiO_2$ | $TiO_2$ | $Al_2O_3$ | $Cr_2O_3$ | FeO | MnO | MgO | CaO | $Na_2O$ | $K_2O$ | F | Cl | $SO_3$ | Cl=O | F=O | Total |
|---|---|---|---|---|---|---|---|---|---|---|---|---|---|---|---|---|---|
| melilite | UCV51, 65/2 | 42.45 | 0.13 | 10.93 | 0 | 0.59 | 0.02 | 7.34 | 34.19 | 4.00 | 0.06 | 0 | 0 | 0.02 | | | 99.73 |
| cancrinite | UCV51, 65/9 | 31.19 | 0 | 26.48 | 0.02 | 0 | 0.04 | 0.04 | 10.04 | 9.89 | 9.09 | 0 | 6.63 | 6.55 | -1.52 | 0 | 98.44 |
| phlogopite | UCV51, 65/14 | 36.64 | 0.89 | 18.25 | 0.09 | 4.11 | 0.05 | 22.18 | 0.43 | 0.07 | 10.08 | 0.05 | 0.02 | 0.05 | -0.00 | -0.02 | 92.87 |
| kalsilite | UCV51, 65/11 | 37.83 | 0 | 31.76 | 0 | 0.16 | 0 | 0 | 0.33 | 0.09 | 28.99 | | | | | | 99.16 |
| | CHX, 62/7 | 38.02 | 0.02 | 31.12 | 0 | 0.89 | 0 | 0.53 | 1.03 | 0.07 | 27.92 | | | | | | 99.60 |
| | VT55, 64/9 | 37.75 | 0 | 30.68 | 0 | 0.50 | 0 | 0.07 | 0.27 | 0.06 | 28.97 | | | | | | 98.30 |
| pyroxene | UCV51, 65/5 | 38.46 | 1.44 | 19.08 | 0.13 | 6.15 | 0.02 | 8.19 | 25.37 | 0.10 | 0 | | | | | | 98.94 |
| | UCV51, 63/71 | 39.11 | 2.09 | 14.69 | 0.26 | 8.85 | 0.11 | 8.59 | 24.87 | 0.10 | 0 | | | | | | 98.67 |
| | CHX, 62/64 | 34.37 | 0.22 | 24.04 | 0.05 | 9.67 | 0.16 | 5.11 | 24.83 | 0.08 | 0 | | | | | | 98.53 |
| | CHX, 62/41 | 33.33 | 0.12 | 23.09 | 0.06 | 13.04 | 0.26 | 3.98 | 24.57 | 0.06 | 0 | | | | | | 98.50 |
| | CHX, 62/14 | 40.88 | 0.02 | 13.22 | 0 | 14.85 | 0.53 | 5.51 | 23.21 | 0.57 | 0 | | | | | | 98.79 |
| | VT55, 52/5 | 36.72 | 0.96 | 12.86 | 0 | 17.60 | 0.79 | 4.90 | 23.52 | 0.08 | 0 | | | | | | 97.43 |
| | VT55, 63/27 | 36.39 | 0.19 | 18.54 | 0.05 | 12.31 | 0.27 | 6.12 | 24.80 | 0.01 | 0 | | | | | | 98.67 |

| | | Structural formulae | Proportion of end members | | | | | |
|---|---|---|---|---|---|---|---|---|
| melilite | UCV51, 65/2 | $(Ca_{1.65}Na_{0.35})(Mg_{0.49}Fe_{0.02}Al_{0.48})(Al_{0.10}Si_{0.90})O_7$ | Na-mel 35 | Gh 12 | Ak 50 | FeAk 2 | | |
| microsommite | UCV51, 65/9 | $(Na_{3.69}K_{2.23}Ca_{0.04})Al_6Si_6O_{24}\bullet(CaCl_2)_{1.07}(CaSO_4)_{0.93}$ | | | | | | |
| phlogopite | UCV51, 65/14 | $K(Mg_{2.44}Fe_{0.25}Al_{1.26}Ti_{0.05})(Al_{0.32}Si_{1.68})O_{10}(OH)_2$ | | | | | | |
| kalsilite | UCV51, 65/11 | $KAlSiO_4$ | | | | | | |
| | CHX, 62/7 | $KAlSiO_4$ | | | | | | |
| | VT55, 64/9 | $KAlSiO_4$ | Di | Hd+Jo | Ae | Ess | CaTs | CaTi |
| pyroxene | UCV51, 65/5 | $Ca(Mg_{0.46}Ti_{0.04}Al_{0.28}Fe^{3+}_{0.19})(Al_{0.56}Si_{1.44})O_6$ | 46 | 0 | 0 | 19 | 28 | 4 |
| | UCV51, 63/71 | $Ca(Mg_{0.49}Fe^{2+}_{0.02}Ti_{0.06}Cr_{0.01}Al_{0.14}Fe^{3+}_{0.26})(Al_{0.52}Si_{1.48})O_6$ | 49 | 2 | 0 | 26 | 14 | 6 |
| | CHX, 62/64 | $Ca(Mg_{0.29}Ti_{0.01}Al_{0.38}Fe^{3+}_{0.31})(Al_{0.70}Si_{1.30})O_6$ | 29 | 0 | 0 | 31 | 38 | 1 |
| | CHX, 62/41 | $Ca(Mg_{0.23}Fe^{2+}_{0.03}Mn_{0.01}Al_{0.32}Fe^{3+}_{0.39})(Al_{0.72}Si_{1.28})O_6$ | 23 | 3 | 0 | 39 | 32 | 0 |
| | CHX, 62/14 | $(Ca_{0.96}Na_{0.04})(Mg_{0.32}Fe^{2+}_{0.20}Mn_{0.02}Al_{0.18}Fe^{3+}_{0.28})(Al_{0.42}Si_{1.58})O_6$ | 32 | 22 | 4 | 28 | 18 | 0 |
| | VT55, 52/5 | $Ca(Mg_{0.29}Fe^{2+}_{0.16}Mn_{0.02}Ti_{0.03}Al_{0.06}Fe^{3+}_{0.42})(Al_{0.54}Si_{1.46})O_6$ | 29 | 18 | 0 | 42 | 6 | 3 |
| | VT55, 63/27 | $Ca(Mg_{0.35}Fe^{2+}_{0.02}Mn_{0.01}Ti_{0.01}Al_{0.22}Fe^{3+}_{0.37})(Al_{0.61}Si_{1.39})O_6$ | 35 | 3 | 0 | 37 | 22 | 1 |

* established by electron-microprobe analysis. Pyroxene components: Di: $CaMgSi_2O_6$, Hd+Jo: $Ca(Fe^{2+},Mn)Si_2O_6$, Ae: $NaFe^{3+}Si_2O_6$, Ess: $CaFe^{3+}AlSiO_6$, CaTs: $Ca^{VI}Al^{IV}AlSiO_6$, and CaTi: $CaTi^{IV}Al_2O_6$.

There are distinctive features of the wollastonite *a* crystals, apart from their large size and their elongate and idiomorphic outline: (i) the twins are rare, invariably planar, and with a small contrast in birefringence between the twinned individuals. (ii) They contain many inclusions. In addition to the inclusions described above and interpreted as relics of the former stage 1 (they cannot be in chemical equilibrium with wollastonite, as will be demonstrated below), and to minerals occurring along fractures and therefore interpreted as later formed (granditic garnet as veinlets, pyrrhotite as scarce large crystals), the most conspicuous inclusions are small but numerous lamellae of magnetite with two or three strictly defined orientations unambiguously related to crystallographic planes of the wollastonite host, mainly cleavages (Fig. 6c). These magnetite lamellae occur only in the central parts of the crystals, in which the boundary with the magnetite-free rim is sharp and idiomorphic. These lamellae may show a tendency to concentrate along a dense network of sinuous lines,

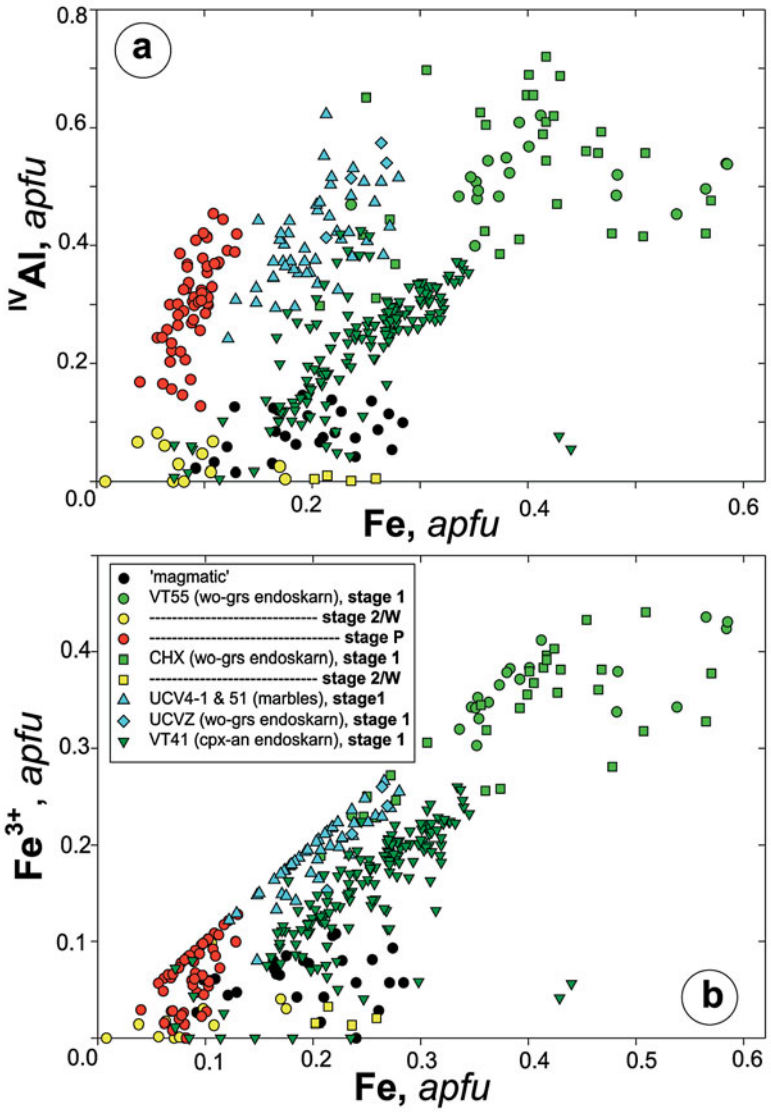


FIG. 5. Compositional ranges of pyroxenes from diorite, endoskarns and marbles. The gradational evolution from the magmatic pyroxene toward Al-rich compositions in endoskarn VT41 is prolonged by the Al- and $Fe^{3+}$-rich pyroxene (stage 1) occurring as inclusions in wollastonite porphyroblasts of endoskarns (CHX, VT55). Diopside (stages 2 and W) is associated with wollastonite and granditic garnet. Later-formed pyroxene of stage P is distinctively poorer in Fe than that of stage 1.

which no doubt represent former fractures. They are accompanied by (Al-free) diopside crystals of the same grain-size, which also show a common orientation. On wollastonite sections showing two perpendicular cleavages, the diopside inclusions appear as squares, the sides of which practically coincide with the cleavage directions of the host wollastonite. Such features suggest epitactic relations between both magnetite and diopside and the host wollastonite, probably corresponding to the exsolution of magnetite and diopside from an earlier single (Fe,Mg)-rich crystal. The later development of the magnetite-free rim was probably accompanied by recrystallization and exsolution of the center, with a Fe-poor composition (Table 3, #53/7). In some cases,

the inner parts of the rim show a ghost-like growth zonation, consisting of strings of tiny inclusions of grossular (Table 3) . Therefore, the second stage of development of the Fe- and Mg-rich wollastonite *a* probably also included this extremely fine-grained granditic garnet.

*Stages of recrystallization in wollastonite–grossular endoskarns: the association wollastonite (b and c) – grossular – diopside*

A first indication that the porphyroblasts of wollastonite *a* do not belong to the same stage as the layered association of grossular (Table 3, #52/28) and fibrous wollastonite (called *wollastonite b*) that constitutes the main part of the groundmass, is that the porphyroblasts *a* are restricted to an outer (exoskarn side) part of the grossular – fibrous wollastonite endoskarn in CHX, whereas in the VT samples they can be observed at any place in the endoskarn.

The porphyroblasts of wollastonite *a* are in part kinked or even broken, and the fibrous layered structure that abuts against these porphyroblasts is deformed, although the individual small crystals of wollastonite do not show any evidence of deformation. This situation is interpreted by invoking simultaneous deformation of the larger and smaller crystals, followed by recrystallization of the smaller grains and of the margins of the porphyroblasts. After deformation, the fractures in wollastonite *a* were invaded by a fine-grained association of wollastonite and grossular (Table 3, #51/35), similar to the association of grossular and fibrous wollastonite *b*. Therefore, the association grossular – wollastonite *b* developed at a comparatively late stage. A moderate degree of recrystallization of the fibrous wollastonite *b* commonly produces prisms larger and stouter than the ordinary needles, but keeping their original orientation.

In sample CHX, as in other samples from the Cornet Hill skarn occurrence, the pyroxene is Al-poor diopside ($Al_2O_3$ usually less than 3 wt.%), developped in association with fibrous wollastonite at the expense of pre-existing pyroxene (Pascal *et al*. 2001). In sample VT55, diopside with a similar composition is observed as irregular modified zones, studded with inclusions of wollastonite, at the periphery of the idiomorphic crystals of clinopyroxene inherited from the magmatic rock (Figs. 7a, b). The relics of the magmatic pyroxene are readily identified through their Fe (0.16–0.30 *apfu*) and Na (0.02–0.04 *apfu*) contents, whereas the modified zones are Fe-poor (less than 0.09 *apfu*) and Na-free.

A third morphological type of wollastonite, *wollastonite c*, corresponds to a more important recrystalliza-

TABLE 3. SELECTED COMPOSITION* OF MINERALS, STAGES 2 AND W (WOLLASTONITE–GARNET ENDOSKARNS)

| | # | $SiO_2$ | $TiO_2$ | $Al_2O_3$ | FeO | MnO | MgO | CaO | $Na_2O$ | $K_2O$ | $P_2O_5$ | $SO_3$ | F | Cl | O=F | Total |
|---|---|---|---|---|---|---|---|---|---|---|---|---|---|---|---|---|
| Wollastonite *a* | *53/7* | 52.37 | 0 | 0.01 | 0.04 | 0.03 | 0.20 | 46.95 | 0.02 | 0 | | | | | | 99.62 |
| Garnet inclusion in wollastonite *b* | *51/35* | 37.24 | 0.49 | 16.28 | 4.79 | 0.09 | 0.45 | 35.93 | 0 | 0 | | | | | | 95.29 |
| Fibrous garnet | *52/28* | 39.86 | 0.19 | 20.61 | 1.57 | 0.07 | 0.46 | 36.56 | 0.02 | 0 | | | | | | 99.43 |
| **Minerals included in wollastonite *c*** | | | | | | | | | | | | | | | | |
| Phlogopite | *51/45* | 39.21 | 0.07 | 18.36 | 0.71 | 0 | 25.02 | 0.58 | 0.01 | 8.75 | | | 0.04 | 0 | -0.02 | 92.76 |
| Ellestadite** | *56/60* | 10.89 | 0.12 | 0 | 0.01 | 0 | 0 | 56.68 | 0.27 | 0.01 | 18.11 | 11.66 | 1.71 | 0.01 | -0.72 | 98.82 |
| Diopside | *53/32* | 53.42 | 0.52 | 1.06 | 3.21 | 0.44 | 16.32 | 25.10 | 0.020 | 0 | 0.05 | | | | | 100.09 |
| Garnet core | *52/52* | 39.09 | 0.66 | 19.56 | 3.06 | 0.12 | 0.48 | 36.26 | 0 | 0 | | | | | | 99.28 |
| rim | *52/51* | 37.74 | 2.34 | 17.61 | 4.41 | 0.02 | 0.77 | 35.83 | 0.01 | 0.04 | | | | | | 98.75 |

| | |
|---|---|
| Wollastonite *a* | $CaSiO_3$ |
| Garnet inclusion in wollastonite *b* | $Ca_{3.08}(Al_{1.53}Fe_{0.32}Mg_{0.05}Ti_{0.03})Si_{2.98}O_{12}$ |
| Fibrous garnet | $Ca_3(Al_{1.84}Fe_{0.10}Mg_{0.05})Si_3O_{12}$ |
| Phlogopite | $K_{0.8}(Mg_{2.7}Fe_{0.04}Al_{1.39})(Al_{0.17}Si_{2.83})O_{12}(OH)_2$ |
| Ellestadite** | $Ca_{5.16}(P_{1.30}Si_{0.93}S_{0.74})O_{12}(OH_{0.55}F_{0.45})$ |
| Diopside | $Ca(Mg_{0.89}Fe^{2+}_{0.08}Fe^{3+}_{0.02}Ti_{0.01})(Al_{0.05}Si_{1.95})O_6$ |
| Garnet core | $Ca_{2.96}Mg_{0.03}(Al_{1.76}Fe_{0.19}Mg_{0.02}Ti_{0.04})Si_{2.98}O_{12}$ |
| rim | $Ca_{2.97}Mg_{0.03}(Al_{1.60}Fe_{0.20}Mg_{0.06}Ti_{0.11})(Fe_{0.08}Si_{2.92})O_{12}$ |

* established by electron-microprobe analysis. ** A hydroxyl-dominant phase intermediate between ellestadite and apatite groups.

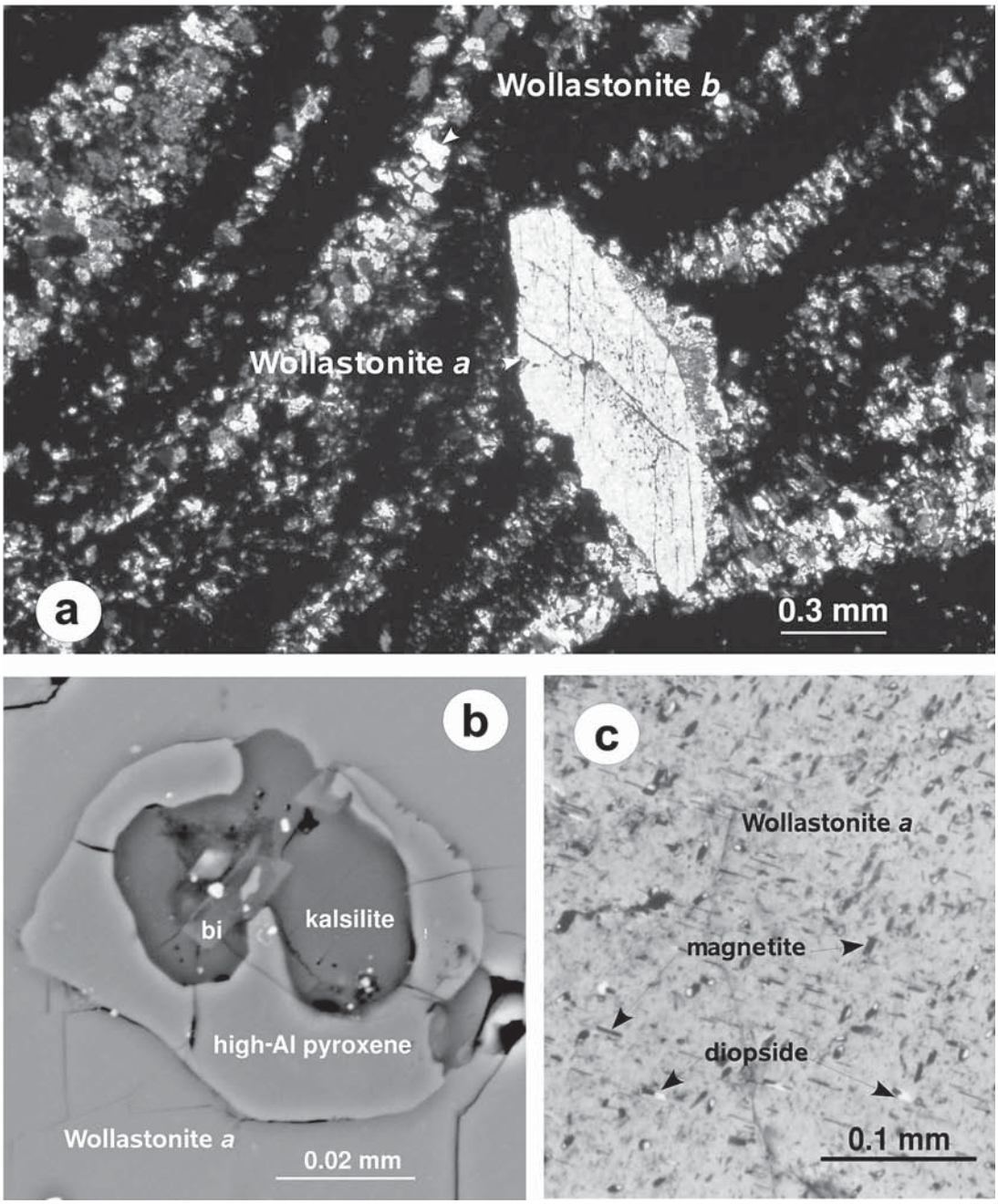


FIG. 6. Wollastonite–grossular endoskarns VT55 and CHX. (a) Photomicrograph of an idiomorphic porphyroblast of wollastonite *a* (stage 2) in the wollastonite–grossular groundmass with its typical striped texture (stage W) (VT55). (b) BSE image of Al-rich pyroxene – kalsilite – phlogopite association (stage 1) included in a porphyroblast of wollastonite *a*. (c) Photomicrograph of magnetite and diopside (white) exsolution-induced features in the center of a porphyroblast of wollastonite *a* (CHX).

tion, producing quite large irregular patches in some places; these patches are randomly oriented, and tend to show in some cases a distribution along a network of veins. Large crystals of more or less Ti-rich (up to 0.14 Ti *apfu*) granditic garnet (Table 3, #52/51, 52/52) occur associated with the veins of wollastonite *c*, and may show an idiomorphic shape in contact with such wollastonite. Wollastonite *c* also includes diopside (Table 3, #53/32) as large crystals with complicated intergrowths along the diopside–wollastonite boundary, and ellestadite (Table 3, #56/60). A few scattered small crystals of phlogopite (Table 3, #53/52) occur

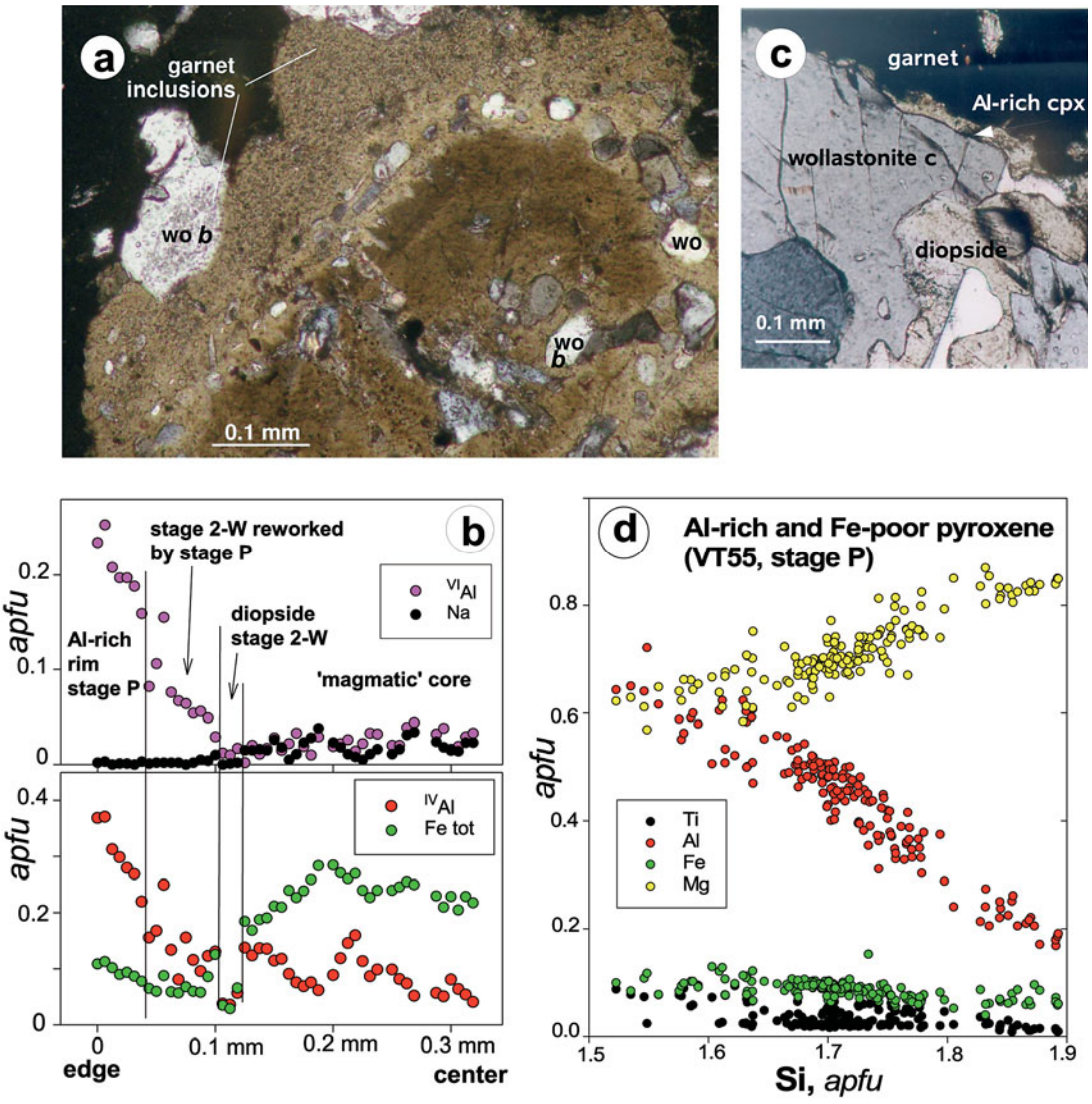


FIG. 7. Al-rich pyroxene (stage P) in endoskarn VT55. (a) Photomicrograph and (b) compositional profile of a zoned pyroxene crystal with a core inherited from the diorite, surrounded by a thin zone of diopside containing inclusions of wollastonite, and by a wide overgrowth of Al-rich pyroxene (stage P) with minute inclusions of grossular, similar to the grossular inclusions in adjacent wollastonite *b*, suggesting that the Al-rich pyroxene replaced wollastonite. (c) Photomicrograph of a vein of wollastonite *c* containing granditic garnet and diopside, with a rim of Al-rich pyroxene between garnet and wollastonite. (d) All measured compositions of pyroxene P define linear trends interpreted by the preservation of the locally pre-existing Al:Mg ratio (see text).

in VT samples, usually in the wollastonite *c* crystals or in the associated garnet. A fine-grained symplectitic intergrowth of perovskite and wollastonite has been observed included in wollastonite *c*, interpreted to be a replacement after titanite.

*Stages of recrystallization in wollastonite–grossular endoskarns: Al-rich and Fe-poor pyroxene*

The peculiarity of the endoskarns VT55–56, compared to CHX and other wollastonite–grossular endoskarns, is the occurrence of Al-rich (but Fe-poor and almost $Fe^{2+}$-free) clinopyroxene in the recrystallized groundmass. The large crystals of pyroxene, with an idiomorphic core inherited from the diorite and partly modified to diopside + wollastonite, show a rim much richer in Al (Table 4, Figs. 7a, b). There is in some cases a discontinuous chemical zoning between center and rim, and invariably a strong continuous increase of Al outward. Close to the endoskarn–exoskarn boundary, rounded crystals with a similar size, entirely studded with inclusions of wollastonite, have the same compositions and zonation as the rim composition just described (Table 4). Some of these crystals, and smaller ones studded or not, occur as a kind of network in the striped layers of fibrous wollastonite. They replace part of the wollastonite and appear along discontinuous cross-cutting veinlets apparently connecting the regions of replaced stripes of wollastonite. In some areas, the wollastonite *b* crystals of the stripes contain numerous tiny rounded inclusions of garnet, and some identical inclusions of garnet, however less numerous, are observed in the pyroxene replacing this wollastonite, suggesting that part of the garnet inclusions was used in development of the pyroxene. Another clear indication of the growth of Al-rich pyroxene at the expense of garnet is the occurrence, in one vein of wollastonite *c*, of delicate local overgrowths of Al-rich pyroxene at several points along the contacts of garnet with wollastonite (Fig. 7c).

That the reverse reaction also occurred is shown by the occurrence, in the same wollastonite vein, of a thin fringe of garnet in a contact between Al-rich pyroxene and diopside crystals. Close to the endoskarn–exoskarn contact, Al-rich and Fe-poor pyroxene occurs associated with perovskite that appears as inclusions in the pyroxene crystals or, in one case, as a veinlet surrounded by pyroxene. In the latter case, the pyroxene occurs as relics in a large crystal of garnet surrounding the perovskite veinlet.

Also, the discontinuous network of pyroxene described above is connected with, and completed by,

TABLE 4. SELECTED COMPOSITIONS* OF PYROXENE WITH Al-RICH OVERGROWTHS (STAGE P) IN VT ENDOSKARNS

| | # | $SiO_2$ | $TiO_2$ | $Al_2O_3$ | FeO | MnO | MgO | CaO | $Na_2O$ | Total |
|---|---|---|---|---|---|---|---|---|---|---|
| magmatic core | *54/179* | 51.26 | 0.51 | 2.05 | 9.03 | 0.48 | 11.66 | 23.65 | 0.51 | 99.20 |
| overgrowth | *54/150* | 43.74 | 0.87 | 14.24 | 3.65 | 0.06 | 10.46 | 25.54 | 0.05 | 98.75 |
| in the striped structure | | | | | | | | | | |
| core | *51/54* | 45.79 | 0.66 | 11.17 | 3.06 | 0.14 | 12.49 | 25.35 | 0.02 | 98.73 |
| rim | *51/55* | 41.28 | 0.86 | 16.35 | 3.76 | 0.05 | 10.11 | 25.28 | 0.02 | 97.71 |
| in perovskite-bearing vein | *51/19* | 40.99 | 3.16 | 14.71 | 3.23 | 0.07 | 11.17 | 25.62 | 0.03 | 98.98 |

| | |
|---|---|
| magmatic core | $Ca_{0.96}Na_{0.04}(Mg_{0.66}Fe^{2+}_{0.24}Mn_{0.01}Ti_{0.01}Al_{0.03}Fe^{3+}_{0.04})(Al_{0.06}Si_{1.94})O_6$ |
| overgrowth | $Ca_{1.02}(Mg_{0.58}Fe^{2+}_{0.04}Ti_{0.02}Al_{0.25}Fe^{3+}_{0.07})(Al_{0.37}Si_{1.63})O_6$ |
| in the striped structure | |
| core | $Ca(Mg_{0.69}Fe^{2+}_{0.01}Ti_{0.02}Al_{0.18}Fe^{3+}_{0.09})(Al_{0.31}Si_{1.69})O_6$ |
| rim | $Ca_{1.02}(Mg_{0.57}Ti_{0.02}Al_{0.27}Fe^{3+}_{0.12})(Al_{0.45}Si_{1.55})O_6$ |
| in perovskite-bearing vein | $Ca_{1.02}(Mg_{0.62}Ti_{0.09}Al_{0.17}Fe^{3+}_{0.10})(Al_{0.48}Si_{1.52})O_6$ |

| | Di | Hd+Jo | Ae | Ess | CaTs | CaTi |
|---|---|---|---|---|---|---|
| magmatic core | 66 | 25 | 4 | 0 | 3 | 1 |
| overgrowth | 58 | 4 | 0 | 7 | 25 | 2 |
| in the striped structure | | | | | | |
| core | 69 | 1 | 0 | 9 | 18 | 2 |
| rim | 57 | 0 | 0 | 12 | 27 | 2 |
| in perovskite-bearing vein | 62 | 0 | 0 | 10 | 17 | 9 |

* established by electron-microprobe analysis.

areas in which very fine interstitial spaces between wollastonite and garnet are filled with serpentine (hardly visible in transmitted light but giving to these minerals an unusual optical relief). In our opinion, the pyroxene network, at first more developed and more continuous, was partially changed to wollastonite + serpentine + grossular granules, which is another instance of transformation of Al-rich pyroxene to garnet.

The pyroxene of this association is invariably Fe-poor and contains up to 16.4% $Al_2O_3$ (Table 4), with a large compositional range defining remarkable linear trends (Fig. 7d), distinct from the compositional field of pyroxene of stage 1 (Fig. 5). The Ti contents of the crystals in the perovskite-bearing veins reach up to 0.1 *apfu* and show a strong correlation with the $^{IV}Al$ contents, whereas the large zoned crystals developed as a modification of the magmatic pyroxene show lower Ti contents, similar to the pyroxene of stage 1. The linear trends of Figure 7d indicate that the composition of pyroxene had only one degree of freedom, *i.e.*, that one chemical parameter was not fixed by the coexisting phases (fluid or minerals), and thus probably was inherited from the local pre-existing composition. The preservation of one chemical parameter in a metasomatic process corresponds to the inert behavior of two components, the ratio of which remains unchanged. In the present case, as Si, Ca and Fe were obviously mobile, the composition of the pyroxene was most probably controlled by the locally inherited ratio Al:Mg. Accordingly, most grains of Al-rich pyroxene of the groundmass were probably produced at the expense of garnet (or other pre-existing Al-bearing minerals), using pre-existing diopside where available as a nucleus and source of Mg. In many cases, such grains clearly replace wollastonite of both types *b* and *c*, and define one or several stages (collectively called *stage P*) somewhat similar to stage 1, which occurred in alternation with the stages characterized by grossular and wollastonite *b* and *c* (collectively called *stage W*).

### *The vesuvianite stage*

Vesuvianite first occurred as a sporadic late-stage mineral, in patches and veins, in some cases developed at the expense of Al-rich pyroxene (of stage P), apparently in equilibrium with wollastonite. Then the rock was transformed to massive vesuvianite, associated with large patches of serpentine. Vesuvianite shows marked but progressive changes in its birefringence within the same patch, which reflect an admixture of submicroscopic grains of calcite. Small well-individualized patches of calcite occur along veinlets, together with serpentine. Where massive, vesuvianite replaces all pre-existing minerals. Only ragged remnants of wollastonite, probably on the way to final disappearance, can still be observed.

## Discussion

### *Thermochemical calculations*

Understanding the complicated succession of processes just described requires the help of calculated conditions of stability of the mineral associations in the system $K_2O$–$Al_2O_3$–CaO–$SiO_2$–$Fe_2O_3$–$H_2O$–$CO_2$. We used the database of Berman (1988) and, for $H_2O$ and for pyroxene and melilite solid-solution properties, the program MELTS (Ghiorso & Sack 1995). In this program, melilite on the join gehlenite–åkermanite is documented from experimental data by Waldbaum (1973) and Charlu *et al.* (1981) (unfortunately, no data are available for Na-bearing melilite). The complex pyroxene solid-solutions in MELTS are described with the model of Sack & Ghiorso (1994a); it has been calibrated against an experimental *ad hoc* database (Sack & Ghiorso 1994b) and also accounts for results of previous experimental studies, such as activity–compositions relations on the join $CaMgSi_2O_6$–$CaAl_2SiO_6$ (Wood 1979), a study of the join $CaMgSi_2O_6$–$Ca(Mg_{0.5}Ti_{0.5}AlSiO_6)$ (Yagi & Onuma 1967), the solubility of $CaFe^{3+}{}_2SiO_6$ in $CaMgSi_2O_6$ (Huckenholz *et al.* 1968) and the miscibility gap in the system $CaMgSi_2O_6$–$CaTiAl_2O_6$–$CaAl_2SiO_6$ (Yang 1975).

The output of MELTS includes the apparent free energy of formation of the minerals and, for solid solutions, the chemical potentials and activities of the end members. However, as a model for pyroxene solid-solutions, Ghiorso & Sack (1995) used a set of end members that does not include the CaTs component. Instead, the monosilicic pyroxene end-members are esseneite ($CaFe^{3+}AlSiO_6$), "buffonite" ($CaMg_{0.5}Ti_{0.5}Fe^{3+}SiO_6$) and "Al-buffonite" ($CaMg_{0.5}Ti_{0.5}AlSiO_6$), the quotation marks indicating that the names of these end members are not sanctioned by the IMA. Therefore, whereas the chemical potentials and activities of Ess and Di in a pyroxene solid-solution were directly obtained from MELTS, the chemicals potentials of the CaTs end-member and component in solid-solution were calculated from those of esseneite (Ess), "buffonite" (Bu) and "Al-buffonite" (AlBu) through the relation CaTs = Ess + AlBu – Bu.

For granditic garnet, we used an ideal two-site mixing model (Perchuk & Aranovich 1979). For the andradite end-member, available thermodynamic data are less accurate than for the other minerals considered. Moreover, no set of values has been checked to be consistent with the data from MELTS for the other $Fe^{3+}$-bearing mineral involved in the calculations, *i.e.*, esseneite. Therefore, we preferred to take the andradite component into account by estimating the constant of the reciprocal equilibrium:

$$\underset{\text{Ess}}{CaFeAlSiO_6} + \tfrac{1}{2}\,\underset{\text{Grs}}{Ca_3Al_2Si_3O_{12}} = \underset{\text{CaTs}}{CaAl_2SiO_6} + \tfrac{1}{2}\,\underset{\text{Adr}}{Ca_3Fe_2Si_3O_{12}} \quad (1)$$

$$K(1) = [a_{Adr}/a_{Grs}]^{0.5} / [a_{Ess}/a_{CaTs}]$$

We have analyzed three different garnet – pyroxene pairs with probable equilibrium textural relationships and calculated the activities of the Ess and CaTs end-members at 700°C (Table 5). The mean value of K(1), 0.074, was used in the phase-diagram calculations.

For every stage of the metasomatic transformations, the calculations were performed using measured compositions of pyroxene, the ones associated with kalsilite at stage 1 and the most Al-rich one at stage P. The compositions of other phases involved in the calculated reactions (melilite, garnet) were taken as corresponding to equilibrium with this pyroxene (note that melilite has never been observed in association with any pyroxene, so that the calculated compositions of melilite have no match among the described minerals). Mineral compositions are indicated in the Figures 8 and 9, and all considered equilibria are listed in Table 6. The fluid pressure, assumed equal to the total pressure, was taken to be 0.75 kbar according to the estimates for the gehlenite skarns of Magureaua Vaţei.

*Conditions of the pre-vesuvianite stages (1, 2, W and P)*

A major difference among the early stages lies in the nature of the Al-bearing mineral, pyroxene at stages 1 and P, garnet at stages 2 and W. The significance of this contrast appears upon consideration of the formal equilibria (2) and (3):

$$\underset{\text{CaTs}}{CaAl_2SiO_6} + 2\,\underset{\text{Wollastonite}}{CaSiO_3} = \underset{\text{Grossular}}{Ca_3Al_2Si_3O_8} \quad (2)$$

$$\underset{\text{Esseneite}}{CaAlFeSiO_6} + 2\,\underset{\text{Wollastonite}}{CaSiO_3} = \underset{\text{Garnet}}{Ca_3AlFeSi_3O_{12}} \quad (3)$$

The Al content of pyroxene at equilibrium with granditic garnet and wollastonite, calculated from eq. (2) and (3) for a garnet $Grs_{80}$, typical for stage W (veins of wollastonite *c* with inclusions of garnet and diopside), ranges from 1.1 wt.% $Al_2O_3$ (0.03 *apfu* $^{IV}Al$) at 700°C to 2.7 wt.% $Al_2O_3$ (0.08 *apfu* $^{IV}Al$) at 800°C, in agreement with the composition of the associated diopside. Therefore, Al-rich pyroxene and wollastonite cannot be an equilibrium association. The pyroxenes of stages 1 and P developed under strongly wollastonite-undersaturated conditions, and the wollastonite-forming fluid at stages 2 and W certainly tended to transform the CaTs and esseneite components of pre-existing pyroxene to granditic garnet according to (2) and (3), as inferred from textural observations. In calcic skarns, as wollastonite expresses the presence of excess silica, the wollastonite–grandite stages are expected to be produced by silica-rich fluids, and the pyroxene stages, by silica-poor fluids.

The desilication of the diorite protolith at *stage 1* is clearly displayed by the reactions observed in sample VT41: the transformation of the albite component of the plagioclase to anorthite corresponds to Ca-for-Na exchange and Si removal; furthermore, the transformation of part of the anorthite to the CaTs end-member of pyroxene (reaction 26, Table 6) corresponds to Si removal. In sample UCV51, the silicates included in calcite (kalsilite and Al- and Fe-rich pyroxene) indicate conditions still more silica-deficient than the mineral association of VT41 (higher CaTs content in pyroxene). The same conditions occur in the endoskarns CHX and VT54–55–56. These associations are characterized by silica activities (with reference to quartz) below $10^{-1.1}$ (Fig. 8).

TABLE 5. EQUILIBRIUM COMPOSITIONS OF GARNET AND PYROXENE

| | garnet | pyroxene | $a_{CaTs}$ | $a_{Ess}$ | K(1) |
|---|---|---|---|---|---|
| Pair 1 | #54/325 | | | | |
| | $Grs_{85}$ | $CaMg_{0.65}Fe^{3+}_{0.16}Al_{0.22}(Al_{0.34}Si_{1.66})O_6$ | 0.20 | 0.46 | 0.072 |
| Pair 2 | #51/28 | | | | |
| | $Grs_{61}$ | $Ca_{1.02}Mg_{0.88}Fe^{3+}_{0.05}Al_{0.04}(Al_{0.09}Si_{1.91})O_6$ | 0.039 | 0.32 | 0.076 |
| Pair 3 | #53/17, 53/20 | | | | |
| | $Grs_{82}$ | $CaMg_{0.82}Fe^{3+}_{0.07}Al_{0.08}Ti_{0.04}(Al_{0.22}Si_{1.78})O_6$ | 0.094 | 0.30 | 0.069 |

TABLE 6. MINERAL EQUILIBRIA REPRESENTED IN THE DIAGRAMS

| | |
|---|---|
| 3 Di + 5 Kls + 3 $CO_2$ + $H_2O$ = 4 Lct + Phl + 3 Cal | 4 |
| 3 Di + 2 CaTs + Kls + Cal + $H_2O$ = 2 Grs + Phl + $CO_2$ | 5 |
| Di + CaTs + Lct + Cal + $H_2O$ = Grs + Phl + $CO_2$ | 6 |
| 3 Di + 1.5 CaTs + 2 Kls + $H_2O$ = Phl + 1.5 Grs + Lct | 7 |
| 2.5 CaTs + Phl = Lct + Di + 2 Spl + 0.5 Grs + $H_2O$ | 8 |
| 0.5 CaTs + Phl + 0.5 Grs = Spl + Kls + 2 Di + $H_2O$ | 9 |
| 5/3 CaTs + Phl + 1/3 $CO_2$ = 5/3 Spl + Lct + 4/3 Di + 1/3 Cal + $H_2O$ | 10 |
| Di + 2 CaTs + Kls = Spl + Gr + Lct | 11 |
| Di + CaTs + Kls + 2 $CO_2$ = Spl + Lct + 2 Cal | 12 |
| 2.5 CaTs + Di + Cal = 1.5 Grs + Spl + $CO_2$ | 13 |
| 2.5 Gh + Ak + 2.5 $CO_2$ = 1.5 Grs + Spl + 2.5 Cal | 14 |
| Gh + $CO_2$ = CaTs + Cal | 15 |
| Ak + $CO_2$ = Di + Cal | 16 |
| Di + 4 CaTs + Gh + Ak =3 Grs + 2 Spl | 17 |
| Di + 3 CaTs = Spl + Grs + An | 18 |
| Di + 4 CaTs + 2 $CO_2$ = Spl + 3 An + 2 Cal | 19 |
| Phl + 4 Wo = Ak + 2 Di + Kls + $H_2O$ | 20 |
| Phl + 4 Wo + 2 Cal = 3 Ak + Kls + $H_2O$ + 2 $CO_2$ | 21 |
| Phl + 4 Wo + $CO_2$ = 3 Di + Kls + Cal + $H_2O$ | 22 |
| Phl + 3 Wo + Lct = 3 Di + 2 Kls + $H_2O$ | 23 |
| 3 Di + Kls + 3 $CO_2$ + $H_2O$ = Phl + 3 Cal + 4 $SiO_2$ | 24 |
| Lct = Kls + $SiO_2$ | 25 |
| An = CaTs + $SiO_2$ | 26 |
| Grs + 2 $CO_2$ = CaTs + 2 Cal + 2 $SiO_2$ | 27 |
| Di + 2 CaTs = Spl + Grs + $SiO_2$ | 28 |
| Ttn = Prv + $SiO_2$ | 29 |

Symbols: Ak: åkermanite, An: anorthite, Cal: calcite, CaTs: Ca-Tschermak component of clinopyroxene, Di: diopside, Gh: gehlenite, Grs: grossular, Kls: kalsilite, Lct: leucite, Prv: perovskite, Phl: phlogopite, Spl: spinel, Ttn: titanite, Wo: wollastonite.

The temperature is constrained by the pyroxene – kalsilite association, stable only above 760°C in VT55, 800°C in CHX. A high pressure of $CO_2$ is necessary to stabilize calcite with Al-rich pyroxene and kalsilite (Figs. 9a, b). Calcite is clearly associated with the minerals of stage 1 in UCV samples, and in endoskarns CHX and VT, the same minerals with the same compositions occur within a few mm from the intrusive contact, *i.e.*, very close to the former limestone. Therefore, the fluid at stage 1 may be considered to have been in equilibrium with calcite. With this assumption, the pressure of $CO_2$ was at least 400 bars in VT and 675 bars in CHX. Taking into account the range 500–750 bars inferred for the fluid pressure at Cornet Hill (Pascal *et al*. 2001), the fluid at stage 1 was probably almost pure $CO_2$.

What we know of *stage 2* is only the comparatively abundant porphyroblasts of wollastonite *a*, inferred to have first crystallized with high Fe and Mg contents, and the tiny crystals of grossular trapped in the overgrowths of the wollastonite porphyroblasts. The extent to which Fe can replace Ca in wollastonite has been experimentally found to be strongly favored by high temperature (Mason 1975), and still more (up to 18 mol.% $FeSiO_3$ at 800°C) can enter the bustamite structure, which becomes stable above 800°C (Rutstein 1971). Several occurrences of ferrobustamite in skarns have been reported, *e.g.*, at the Kagata mine, Japan (Shimazaki & Yamanaka 1973) and Skye (Tilley 1948, Rapoport & Burnham 1973). Fe-rich wollastonite has also been reported from melilite-bearing paralavas (Melluso *et al*. 2003). No experimental data are available about the Mg-for-Ca substitution in wollastonite, but relatively high contents of Mg (0.17 *apfu*) as well as Fe (0.20 *apfu*) have been found in wollastonite from a contact zone ("hydridized pyroxenite") developed between a dolerite plug and the surrounding chalk at Carneal, Ireland (Sabine 1975). Therefore, the wollastonite *a* most probably formed under high-temperature conditions similar to those of stage 1.

According to equations (2) and (3), the Al-rich pyroxene of stage 1 included in these crystals is in strong disequilibrium with wollastonite and should not have been preserved (indeed, no such pyroxene was found outside the crystals of wollastonite *a*), unless it was quickly protected from the wollastonite-forming medium by rapid growth of the host wollastonite, so that the contacts between pyroxene inclusions and the host crystal are devoid of any reaction (except perhaps for the growth of the tiny crystals of biotite shown in Fig. 6b). Such a rapid growth indicates a strong oversaturation with respect to wollastonite, which could only result from the influx of a Si-rich fluid or liquid into a calcite-bearing rock containing minerals of stage 1. At the stage 1, this rock was probably a network of silicate veinlets in calcite, such as in UCV4–1 or UCV51. The porphyroblasts of wollastonite that replaced calcite have a remarkable idiomorphic shape, although in some

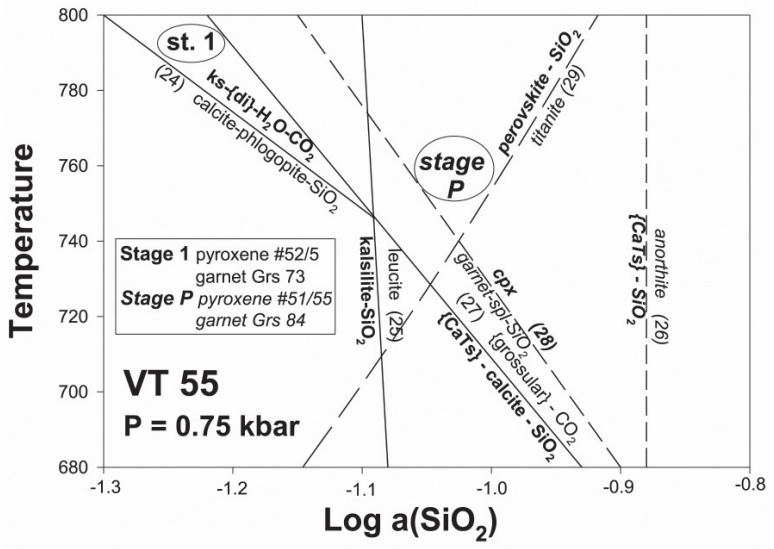


FIG. 8. Conditions of temperature and $SiO_2$ activity (with reference to quartz) for Al-rich pyroxene at VT55. Stage-1 pyroxene associated with kalsilite requires both a high temperature and a strong undersaturation in silica. Stage-P pyroxene (italics) may be formed under lower temperature. Pyroxene compositions are listed in Tables 2 and 4; reactions (braces indicate an end member in a solid-solution series) are listed in Table 6.

places they are partly broken; we suggest that they are more likely to have crystallized by reaction with calcite in a silicate-rich fluid phase, such as a pegmatite-forming fluid, prior to the groundmass, than to simply result from a metasomatic process due to a vapor phase alone. Whatever its nature, the fluid was certainly $CO_2$-poor, in accordance with a possibly magmatic origin, because silica cannot be transported in large amounts by a $CO_2$-rich, $H_2O$-poor fluid (Novgorodov 1975).

The stages labeled *W* correspond to repeated recrystallization of the skarn produced by stages 1 and 2, to give the grossular – fibrous wollastonite – diopside association. The same association also is developed at the expense of the adjacent igneous rock on a scale of one centimeter or so in sample CHX, as inferred from the presence of a wollastonite – grossular – diopside zone devoid of wollastonite *a* at the contact of the monzodiorite. A lower temperature of equilibration, compared to the earlier stages, is indicated by the exsolution of magnetite and diopside from porphyroblasts of wollastonite *a* (Fig. 6c).

As phlogopite is the only K-bearing mineral observed outside the wollastonite *a* porphyroblasts, we assume that phlogopite was stable, which constrains the $CO_2$ pressure to a value below 100 bars (Fig. 9c), in accordance with the fact that this kind of endoskarn is typically found as the inner zone of a zoned gehlenite-bearing endoskarn, characterized by a low pressure of $CO_2$.

The stage(s) labeled *P* have been defined as the re-appearance of Al-rich (but Fe-poor) pyroxene at the expense of grossular and wollastonite in the VT samples. The lower stability-limit of the pyroxene is 670°C for the most Al-rich compositions (Fig. 9d). Phlogopite in association with pyroxene is stable up to quite high values of $CO_2$ pressure (hence low $H_2O$ pressure), instead of kalsilite as in stage 1, because the low Fe-contents of the pyroxene result in higher mole fractions of CaTs and Di, which shift the pyroxene–kalsilite field toward higher temperature.

The low activity of silica (Fig. 8), consistent with the stability of perovskite, suggests chemical conditions more or less similar to those of stage 1, *i.e.*, silica-poor and probably $CO_2$-rich. The absence of calcite is not surprising in view of the quite high pressure of $CO_2$ necessary to stabilize calcite with such pyroxene (Fig. 9d).

*The early calcite–magma reaction*

In all three occurrences reported, Cornet Hill, Upper Cerboaia Valley and Ciclova, relics of stage 1 have characteristics consistent with the development of a Si-depleted endoskarn a few centimeters thick, at the margins and apophyses of the intrusive bodies, at very high temperature and by a $CO_2$-dominated fluid. Although the presence of $CO_2$-rich fluids is not *a priori* surprising in skarns, pyroxenes such as those reported here are uncommon. The wollastonite – anorthite – grossular – pyroxene nodule from La Soufrière, with a composition of pyroxene typical of our pyroxene 1 (Fig. 1), is suggested to have formed by "high temperature reaction between magma and calcareous wallrock" (Arculus & Wills 1980). In skarn ejecta from Monte Somma – Vesuvius, pyroxene (associated with abundant phlogopite, spinel and, occasionally, olivine) is reported to reach 20 wt% $Al_2O_3$ (Hermes & Cornell 1983). A fluid-inclusion study of these minerals (Belkin *et al.* 1985) revealed the presence of melt inclusions indicating a temperature of crystallization of about 1000°C, and $CO_2$ inclusions with a variable density but no optically detectable $H_2O$. The presence of such fluids agrees with our conclusion that the Al-rich pyroxenes formed at very high temperature in the presence of a $CO_2$-dominated fluid. This fluid may be considered to have resulted from the reaction of calcite with the silicate melt at the time of magma emplacement, and to have caused the crystallization of aluminous clinopyroxene ± calcic plagioclase (Joesten 1977, Owens 2000) that, owing to reworking by the fluid, gave the stage-1 endoskarns.

*Origin of the pyroxene (± kalsilite) veinlets in marble*

In the marble (UCV samples) close to what may be interpreted as a former intrusive contact, the peraluminous-clinopyroxene-bearing mineral association of the veinlets corresponds to the recrystallization of a pre-existing material by the fluid of stage 1, with an inert behavior of most chemical components (except Ca and Si), as inferred from the irregular composition of the pyroxene crystals of stage 1. Therefore, the protolith contained not only Mg, Fe, Al and appreciable Ti, but also some Cr (the $Cr_2O_3$ content of the pyroxene is commonly higher than 0.1 wt.% and reaches up to 0.26 wt.%). Cr-bearing minerals have been found in the monzodiorite of Cornet Hill (orthopyroxene with up to 0.85 wt.% $Cr_2O_3$), and in the Oraviţa–Ciclova complex, which contains more-or-less reacted phenocrysts (Cr-rich clinopyroxene with up to 1.1 wt% $Cr_2O_3$ and chromite inclusions, Cr-bearing pargasitic hornblende: Katona 2004) corresponding to crystallization from an $H_2O$-rich mafic melt. The existence of a mafic component in the Oraviţa–Ciclova intrusive complex is also displayed by the occurrence of gabbrodiorites in the area close to the gehlenite skarns at Oraviţa, and a succession of basic, then more differentiated magmas has been observed in two other banatitic complexes, Bocsa and Surduc (Russo-Sandulescu *et al.* 1976, Russo-Sandulescu & Berza 1979), located near Oraviţa (Fig. 2).

Therefore, the veinlets containing the peraluminous pyroxene probably derive from former veinlets of mafic, Cr-bearing magma, emplaced in the limestone prior to the main intrusive body that developed the $CO_2$-producing contact-metamorphic reactions described

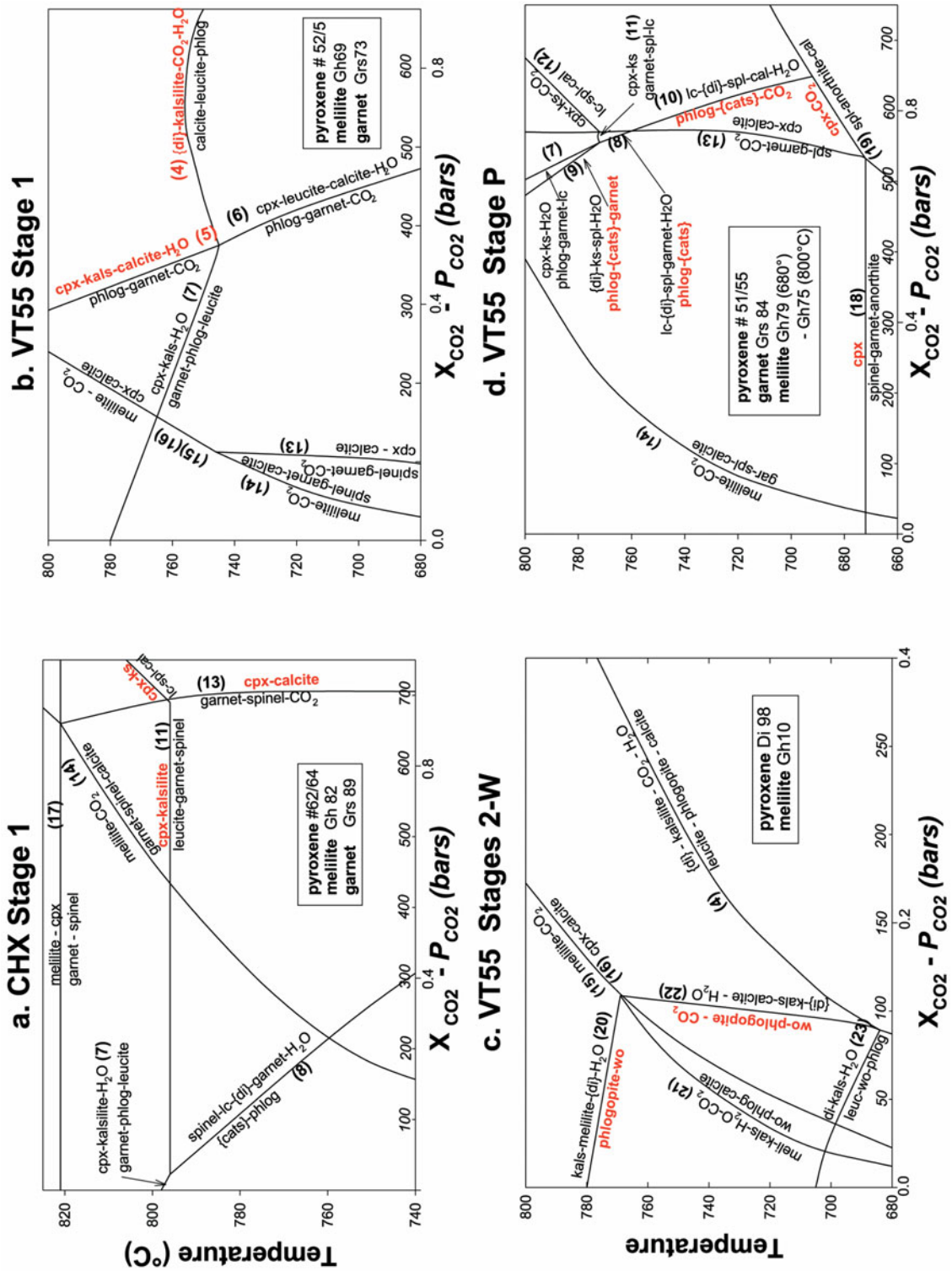
b. VT55 Stage 1
pyroxene # 52/5
melilite Gh69
garnet Grs73
(4) {di}-kalsilite-CO2-H2O
calcite-leucite-phlog
(6) cpx-leucite-calcite-H2O
phlog-garnet-CO2
cpx-kals-calcite-H2O (5)
phlog-garnet-CO2
(7)
cpx-kals-H2O
garnet-phlog-leucite
melilite - CO2
cpx-calcite
(15)/(16)
(13)
cpx - calcite
spinel-garnet-CO2
(14)
melilite-CO2
XCO2 - PCO2 (bars)
d. VT55 Stage P
pyroxene # 51/55
garnet Grs 84
melilite Gh79 (680°)
- Gh75 (800°C)
(10) lc-{di}-spl-cal-H2O
cpx-ks
garnet-spl-lc
(11)
lc-spl-cal (12)
cpx-ks-CO2
cpx-CO2
phlog-{cats}-CO2
cpx-calcite
(7)
(8)
(9)
spl-garnet-CO2 (13)
spl-anorthite-cal
cpx-ks-H2O
phlog-garnet-lc
{di}-ks-spl-H2O
phlog-{cats}-garnet
lc-{di}-spl-garnet-H2O
phlog-{cats}
(14)
melilite-CO2
gar-spl-calcite
cpx
(18)
spinel-garnet-anorthite
XCO2 - PCO2 (bars)
a. CHX Stage 1
pyroxene #62/64
melilite Gh 82
garnet Grs 89
cpx-ks
lc-spl-cal
(13) cpx-calcite
garnet-spinel-CO2
(11)
leucite-garnet-spinel
cpx-kalsilite
(14)
melilite-CO2
garnet-spinel-calcite
(17)
melilite - cpx
garnet - spinel
cpx-kalsilite-H2O (7)
garnet-phlog-leucite
spinel-lc-{di}-garnet-H2O
{cats}-phlog
(8)
Temperature (°C)
XCO2 - PCO2 (bars)
c. VT55 Stages 2-W
pyroxene Di 98
melilite Gh10
{di} - kalsilite - CO2 - H2O
leucite - phlogopite - calcite
(4)
(15) melilite-CO2
(16) cpx-calcite
{di}-kals-calcite - H2O (22)
wo-phlogopite - CO2
kals-melilite-{di}-H2O (20)
phlogopite-wo
mell-kals-H2O-CO2 (21)
wo-phlog-calcite
di-kals-H2O (23)
leuc-wo-phlog
Temperature
XCO2 - PCO2 (bars)

above. This interpretation provides an explanation of the intriguing fact that wollastonite–grossular endoskarns such as CHX and VT55, which unquestionably preserve some features inherited from a magmatic rock, enclose remnants of mineral associations previously entirely surrounded by marble.

*Calcium contamination of the magma*

A possible influence of the calcite–magma reaction on the magma itself, in addition to the precipitation of Al-rich pyroxene, cannot be directly observed because all intrusive contacts have been later modified, but may be inferred from more or less similar processes described in literature. A classical example of reactions between olivine dolerites and limestones (chalk) is that of Scawt Hill (Tilley & Harwood 1931). In the immediate vicinity of the chalk contact, the basalt progressively grades into a vesiculated, almost plagioclase-free, Mg-rich pyroxenite, interpreted as resulting from reaction with limestone, leaving a melt enriched in sodium and iron, which corresponds to (Mg-poor) augite – plagioclase rocks. Further assimilation of lime led to the progressive disappearance of plagioclase in favor of nepheline and the CaTs component of pyroxene (nepheline – plagioclase – Al-rich titanian augite rocks), and to the appearance of melilite. Another instance of melilite and Al-rich pyroxene appearing through assimilation of lime by a silicate melt, also an alkaline basalt, has been reported from the encounter of a basaltic flow with corals at La Réunion (Havette *et al*. 1982).

Interestingly, the melilite ($Ak_{52}Na\text{-}mel_{35}Gh_{12}$) observed in UCV51 as inclusions in calcite very close to the silicate veins compositionally resembles the melilite of contaminated dolerites (except for a lower Fe:Mg ratio) and, more generally, plots in the field of magmatic melilite (Fig. 10); it is quite different from that of the Na-poor, gehlenite-rich melilite from skarns and from the melilite calculated as corresponding to equilibrium with the Al-rich pyroxene of stage 1 ($Gh_{82}$ in CHX, $Gh_{69}$ in VT55). The former presence of nepheline in UCV51 is suggested by the abundance of thomsonite, a common product of alteration of nepheline, and the presence of an inclusion of primary microsommite (Fig. 4b) in adjacent calcite. The mafic character of the magmatic material in UCV51, inferred above, suggests that the analogy with Scawt Hill deserves to be considered, and that the Na-rich melilite of UCV51 could be an untransformed witness of former silica-undersaturated magmatic veinlets, resulting from the reaction of the melt with calcite. The case of UCV51 is perhaps similar to that described by Brouwer (1946), of veinlets of glassy leucite phonolite and trachyte occurring in blocks of melilite-bearing skarn ejected by the andesitic volcano Merapi, in Indonesia.

*Relation of the wollastonite (±gehlenite) to the calcite–magma reaction*

The development of wollastonite (stages 2 and W) started after stage 1, but still at quite a high temperature. It overprinted stage 1 everywhere at Cornet Hill, but not at Ciclova, where wollastonite-free skarns are observed in contact with diorite. Gehlenite, which occurs at Magureaua Vaţei very close to the rocks described in this paper and usually in close association with wollastonite, probably belongs to the same stages. A similar association of (Fe,Mg)-rich wollastonite with gehlenite has been described from the high-grade contact metamorphic aureole at Carneal, as noted above. However, the mode of formation of the gehlenite is beyond the scope of the present study.

The porphyroblasts of wollastonite *a* have been interpreted as the result of a reaction between a pegmatite-forming liquid or fluid and incorporated fragments of calcite (some of them containing relics of the mineral association of stage 1). If this interpretation is correct, the assumed reaction is the same kind of process as described above for the stage 1, producing different minerals owing to the different composition of the liquid or fluid, richer in silica and especially in $H_2O$. Upon reaction with calcite, its feldspar and quartz components were transformed to the wollastonite–grossular association. In the same way as the calcite–magma reaction of stage 1, this reaction released $CO_2$ and consumed silica, which resulted in a progressive shift of the local chemical conditions from an excess of

FIG. 9. Conditions of temperature and $CO_2$ pressure at stages 1, 2, W and P. Pyroxene compositions are listed in Tables 2, 3 and 4. Garnet and melilite compositions indicated in the diagrams are calculated assuming equilibrium with pyroxene. Reactions (braces indicate an end member in a solid-solution series) are listed in Table 6. (a, b) Stage 1. Temperature is constrained by the Al-rich pyroxene – kalsilite association, stable only above 800°C in CHX and 760°C in VT55. A high pressure of $CO_2$, at least 675 bars in CHX and 400 bars in VT, is necessary to stabilize calcite with Al-rich pyroxene and kalsilite. Taking into account the range 500–750 bars inferred for the fluid pressure at Magureaua Vaţei (Pascal *et al*. 2001), the fluid of stage 1 was probably almost pure $CO_2$. (c) Stages 2 and W. The wollastonite–phlogopite association is stable under a $CO_2$ pressure below 100 bars and temperature below 780°C. These conditions (point kalsilite – phlogopite – calcite – pyroxene – melilite – wollastonite) strongly depend on the total pressure on the fluid phase and would be shifted toward higher values at higher pressure. (d) Stage P. The lower temperature of stability (670°C) of the most Al-rich pyroxene corresponds to its decomposition into spinel + garnet + anorthite, or, at very high $CO_2$ pressure, spinel + anorthite + calcite. Phlogopite in association with pyroxene is stable up to high $CO_2$ pressures (hence low $H_2O$ pressure) (eq. 8, 9, 10), instead of kalsilite as in stage 1, because the low Fe-contents of the pyroxene result in higher CaTs and Di mole fractions, which shift the pyroxene–kalsilite field toward higher temperature (eq. 7).

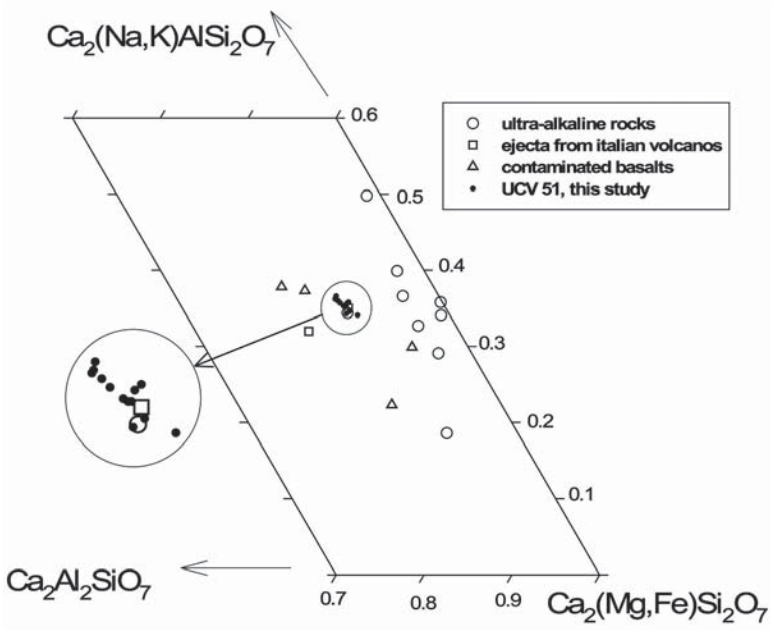


FIG. 10. Compositions of melilite from marble UCV51, contaminated basalts from Scawt Hill (Tilley & Harwood 1931), Carneal (Sabine 1975), and La Réunion (Havette *et al.* 1982), ejected blocks from Vesuvius and Albano, and various melilite-bearing rocks from ultra-alkaline complexes (data taken from Deer *et al.* 1986). The two compositions close to melilite UCV51 are from the Albano (Italy) ejected block and Oka ultra-alkaline complex, Quebec.

silica (crystallization of wollastonite, stages 2 and W) to silica-deficient, $CO_2$-rich conditions more-or-less similar to those of stage 1 (resorption of wollastonite and enrichment of pyroxene in Al, stage P), in agreement with the observed compositional evolution of the pyroxene crystals and their tendency to replace wollastonite.

The inferred high temperature of crystallization of the wollastonite *a*, as well as its limited amount, suggest that stage 2 (at least) was not related to the end of the major magmatic stage. A possible reason for a strongly differentiated liquid to be produced at an unusually high temperature might be an influx of the $CO_2$-rich, Ca-bearing fluid of stage 1 into the magma. The expected effect of such a fluid is to enhance the crystallization of the magma and to raise its solidus temperature, in accordance with the ubiquitous presence, at the intrusive contacts, of veins and patches of alkali feldspar (invariably the last mineral to crystallize from the magma) with very prominent perthitic intergrowths or, where not unmixed, compositions indicating crystallization temperatures in the range 800–820°C (Pascal *et al.* 2001, Katona 2004). The major postmagmatic hydrothermal stage started later, with the development of the normal vesuvianite-dominant skarn association.

## CONCLUDING REMARKS

One of the problems addressed in previous contributions on high-temperature skarns was the apparent evidence for an important degree of transport, by fluids, of elements usually considered to be inert because of their limited solubility, such as Al (*e.g.*, Burnham 1959). We believe that skarn formation actually involves two groups of episodes, among which only the second, entirely postmagmatic, is dominated by fluid (vapor) transport and produces large amounts of vesuvianite, calcic garnet and other calcium-bearing silicates most commonly found in skarns. These postmagmatic processes overprint the earlier, synmagmatic ones, to such an extent that information about the earlier episodes is almost lost. The peculiarity of "high-temperature skarns" is perhaps the (partial) preservation of those earlier processes that involved the magmas and produced, through a combination of high temperature and efficient release of $CO_2$, CaTs-rich pyroxene as the most typical mineral, but involved little transport of matter by fluids *sensu stricto*. The magmatic episodes included a progressive emplacement of melts, with early ($H_2O$-rich) veins that were later incompletely invaded by larger bodies (possibly different in composition), so

that the present boundary between skarns and slightly modified magmatic rock does not correspond to the limit of the material of magmatic origin. The zone of limestone + magmatic veins is most probably the protolith of those intriguing skarns that look like exoskarns and seem to have involved considerable addition not only of Si, but also of Al and, in some cases, Mg and Ti. Their conditions of formation correspond to the climax of contact metamorphism and associated metasomatism, under the influence of a magma possibly different, and certainly emplaced later, than the basic to intermediate melts that originally crystallized as silicate veins in the marble.

## Acknowledgements

This study could not have been achieved without the special efficiency of the Camparis team, Claudine Richard, Omar Boudouma and Michel Fialin, in performing mineral analyses and imaging. They are gratefully acknowledged. We also thank R. Abart, R.F. Martin, and M.F. Taner for comments and suggestions that helped us to improve an earlier version of this manuscript, and C. Wagner for a careful reading of the present text.

## References

Arculus, R.J. & Wills, K.J.A. (1980): The petrology of plutonic blocks and inclusions from the Lesser Antilles island arc. *J. Petrol.* **21**, 743-799.

Belkin, H.E., De Vivo, B., Roedder, E. & Cortini, M. (1985): Fluid inclusion geobarometry from ejected Mt. Somma – Vesusius nodules. *Am. Mineral.* **70**, 288-303.

Berman, R.B. (1988): Internally-consistent thermodynamic data for minerals in the system $Na_2O$–$K_2O$–CaO–MgO–FeO–$Fe_2O_3$–$Al_2O_3$–$SiO_2$–$TiO_2$–$H_2O$–$CO_2$. *J. Petrol.* **29**, 445-522.

Berza, T., Constantinescu, E. & Vlad, S.N. (1998): Upper Cretaceous magmatic series and associated mineralizations in the Carpathian-Balkan orogen. *Res. Geol.* **48**, 291-306.

Blander, M. & Fuchs, L.H. (1975): Calcium–aluminium-rich inclusions in the Allende meteorite: evidence for a liquid origin. *Geochim. Cosmochim. Acta* **39**, 1605-1619.

Bobrievich, A.P., Bondarenko, M.N., Gunashev, M.A., Krasor, A.M. & Smirnov, G.L. (1959): *The Diamond Deposits of Yakutia*. Gosgeoltekhisdat, Moscow, Russia (in Russ.).

Brouwer, H.A. (1946): The association of alkali rocks and metamorphic limestone in a block ejected by the volcano Merapi (Java). *K. Akad. Wetensch. Amsterdam Verh.* **48**, 166-189.

Burnham, C.W. (1959): Contact metamorphism of magnesian limestones at Crestmore, California. *Geol. Soc. Am., Bull.* **70**, 879-928.

Charlu, T.V., Newton, R.C. & Kleppa, O.J. (1981): Thermochemistry of synthetic $Ca_2Al_2SiO_7$ (gehlenite) – $Ca_2MgSi_2O_7$ (akermanite) melilites. *Geochim. Cosmochim. Acta* **45**, 1609-1617.

Codarcea, A. (1932): Etude géologique et pétrographique de la région Ocna de Fier – Bocsa Montana (Roumanie). *An. Inst. Géol. Rom.* **XV**, 435 p.

Constantinescu, E., Ilinca, G. & Ilinca, A. (1988): Contributions to the study of the Oraviţa–Ciclova skarn occurrence, southwestern Banat. *D.S. Inst. Geol. Geofiz.* **72–73/2,** 27-45.

Cosca, M.A. & Peacor, D.R. (1987): Chemistry and structure of esseneite ($CaFe^{3+}AlSiO_6$), a new pyroxene produced by pyrometamorphism. *Am. Mineral.* **72**, 148-156.

Cundari, A. (1982): Petrology of clinopyroxenite ejecta from Somma–Vesuvius and their genetic implications. *Tschermaks Mineral. Petrogr. Mitt.* **30**, 17-35.

Dana, E.S. (1915): *Descriptive Mineralogy* (6th ed.). John Wiley & Sons, New York, N.Y.

Deer, W.A., Howie, R.A. & Zussman, J. (1978): *Rock-Forming Minerals*. **2A**. *Single-Chain Silicates* (2nd ed.). Longman, London, U.K.

_____, _____ & _____ (1986): *Rock-Forming Minerals*. **1B**. *Disilicates and Ring Silicates* (2nd ed.). Longman, London, U.K.

Dodd, R.T. (1971): Calc-aluminous insets in olivine of the sharps chondrite. *Mineral. Mag.* **38**, 451-458.

Dupont, A., Vander Auwera, J., Pin, C., Marincea, Ş. & Berza, T. (2002): Trace element and isotope (Sr,Nd) geochemistry of porphyry- and skarn-mineralizing Late Cretaceous intrusions from Banat, western South Carpathians, Romania. *Mineral. Deposita* **37**, 568-586.

Foit, F.F., Jr, Hooper, R.L. & Rosenberg, P.E. (1987): An unusual pyroxene, melilite and iron oxide mineral assemblage in a coal-fire buchite from Buffalo, Wyoming. *Am. Mineral.* **72**, 137-147.

Gasparik, T. (1984): Experimentally determined stability of clinopyroxene + garnet + corundum in the system CaO–MgO–$Al_2O_3$–$SiO_2$. *Am. Mineral.* **69**, 1025-1035.

Ghiorso, M.S. & Sack, R.O. (1995): Chemical mass transfer in magmatic processes. IV. A revised and internally consistent thermodynamic model for the interpolation and extrapolation of liquid–solid equilibria in magmatic systems at elevated temperatures and pressures. *Contrib. Mineral. Petrol.* **119,** 197-212.

GROSS, S. (1977): The mineralogy of the Hatrurim Formation, Israel. *Geol. Surv. Israel, Bull.* **70**, 1-80.

HAVETTE, A., CLOCHIATTI, R., NATIVEL, P. & MONTAGGIONI, L. (1982): Une paragénèse inhabituelle à fassaïte, mélilite et rhönite dans un basalte alcalin contaminé au contact d'un récif corallien (Saint-Leu, Ile de la Réunion). *Bull. Minéral.* **105**, 364-375.

HAZEN, R.M. & FINGER, L.W. (1977): Crystal structure and compositional variation of Angra Dos Reis fassaite. *Earth Planet. Sci. Lett.* **35**, 357-362.

HERMES, O.D. & CORNELL, W.C. (1981): Quenched crystal mush and associated magma compositions as indicated by intercumulus glasses from Mt Vesuvius, Italy. *J. Volcanol. Geotherm. Res.* **9**, 133-149.

_____ & _____ (1983): The significance of mafic nodules in the ultra-potassic rocks from Central Italy – reply. *J. Volcanol. Geotherm. Res.* **16**, 166-172.

HIJIKATA, K. (1968): Unit-cell dimensions of the clinopyroxenes along the join $CaMgSi_2O_6$–$CaFe^{3+}AlSiO_6$. *J. Fac. Sci. Hokkaido Univ.* **14**(2), 149-157.

_____ & ONUMA, K. (1969): Phase equilibria of the system $CaMgSi_2O_6$–$CaFe^{3+}AlSiO_6$ in air. *Jap. Assoc. Mineral. Petrol. Econ. Geol. J.* **62**, 209-217.

HUCKENHOLZ, H.G. (1973): The origin of fassaitic augite in the alkali basalt suite of the Hocheifel area, western Germany. *Contrib. Mineral. Petrol.* **40**, 315-326.

_____, SCHAIRER, J.F. & YODER, H.S., JR. (1968): Synthesis and stability of ferri-diopside. *Carnegie Inst. Wash. Yearb.* **66**, 335-347.

ILINCA, G., MARINCEA, Ş, RUSSO-SANDULESCU, D., IANCU, V. & SEGHEDI, I. (1993): Mineral occurences in southwestern Banat. *Rom. J. Mineral.* **74**, 1-39.

JAMTVEIT, B., DAHLGREN, S. & AUSTRHEIM, H. (1997): High-grade contact metamorphism of calcareous rocks from the Oslo rift, southern Norway. *Am. Mineral.* **82**, 1241-1254.

JOESTEN, R. (1977): Mineralogical and chemical evolution of contaminated igneous rocks at a gabbro–limestone contact, Christmas Mountains, Big Bend region, Texas. *Geol. Soc. Am., Bull.* **88**, 1515-1529.

KATONA, I. (2004): *Formation de skarns et histoire de la cristallisation magmatique en bordure d'une intrusion monzodioritique* (*Ciclova–Oraviţa, Banat, Romanie*). Thèse de doctorat, Université Catholique de Louvain, Louvain-la-Neuve, Belgium.

_____, PASCAL, M.-L., FONTEILLES, M. & VERKAEREN, J. (2003): The melilite ($Gh_{50}$) skarns of Oraviţa, Banat, Romania: transition to gehlenite ($Gh_{85}$) and to vesuvianite. *Can. Mineral.* **41**, 1255-1270.

LOVERING, J.F. & WHITE, A.J.R. (1969): Granulitic and eclogitic inclusions from basic pipes at Delegate, Australia. *Contrib. Mineral. Petrol.* **21**, 9-52.

MARINCEA, Ş., BILAL, E., VERKAEREN, J., PASCAL, M.-L. & FONTEILLES, M. (2001): Superposed parageneses in the spurrite-, tilleyite- and gehlenite-bearing skarns from Cornet Hill, Apuseni Mountains, Romania. *Can. Mineral.* **39**, 1435-1453.

MASON, B. (1975): Compositional limits of wollastonite and bustamite. *Am. Mineral.* **60**, 209-212.

MELLUSO, L., CONTICELLI, S., D'ANTONIO, M., MIRCO, N.P. & SACCANI, E. (2003): Petrology and mineralogy of wollastonite- and melilite-bearing paralavas from the Central Apennines, Italy. *Am. Mineral.* **88**, 1287-1299.

NEUBAUER, F. (2002): Contrasting late Cretaceous with Neogene ore provinces in the Alpine – Balkan – Carpathian – Dinaride collision belt. *In* the Timing and Location of Major Ore Deposits in an Evolving Orogen (D.J. Blundell, F. Neubauer & A. von Quadtz, eds.). *Geol. Soc., Spec. Publ.* **24**, 81-102.

NOVGORODOV, P.G. (1975): Solubility of quartz in $H_2O$–$CO_2$ mixtures at 700°C and pressures of 3 and 5 kbar. *Geochem. Int.* **12**(5), 122-126.

NUMANO, T. (1978): Geological and geochemical studies on gehlenite–spurrite skarns at Kushiro, the town of Tojo, Hiroshima Prefecture. I. Geology and petrochemistry of the skarn region. *Bull. School Educ., Okayama Univ.* **49**, 25-47 (in Japanese).

_____ (1979): Geological and geochemical studies on gehlenite–spurrite skarns at Kushiro, the town of Tojo, Hiroshima Prefecture. II. Occurrences of gehlenite skarns at the Hirata outcrop. *Bull. School Educ., Okayama Univ.* **50**, 257-282 (in Japanese).

ONUMA, K., AKASAKA, M. & YAGI, K. (1981): The bearing of the system $CaMgSi_2O_6$–$CaAl_2SiO_6$–$CaFeAlSiO_6$ on fassaitic pyroxene. *Lithos* **14**, 173-182.

OWENS, B.E. (2000): High-temperature contact metamorphism of calc-silicate xenoliths in the Kiglapait Intrusion, Labrador. *Am. Mineral.* **85**, 1595-1605.

PASCAL, M.-L., FONTEILLES, M., VERKAEREN, J., PIRET, R. & MARINCEA, Ş. (2001): The melilite-bearing high-temperature skarns of the Apuseni mountains, Carpathians, Romania. *Can. Mineral.* **39**, 1405-1434.

PEACOR, D.R. (1967): Refinement of the crystal structure of a pyroxene of formula $M_IM_{II}(Si_{1.5}Al_{0.5})O_6$. *Am. Mineral.* **52**, 31-41.

PERCHUK, L.L. & ARANOVICH, L.Y. (1979): Thermodynamics of minerals of variable composition: andradite–grossularite and pistacite–clinozoisite solid solutions. *Phys. Chem. Minerals* **5**, 1-14.

POUCHOU, J.L. & PICHOIR, F. (1985): 'PAP' (Φ–ρ–Z) correction procedure for improved quantitative microanalysis. *In* Microbeam Analysis (J.T. Armstrong, ed.). San Francisco Press, San Francisco, California (104-106).

POVODEN, E., HORACEK, M. & ABART, R. (2002): Contact metamorphism of siliceous dolomite and impure limestones from the Werfen formation in the Eastern Monzoni contact aureole. *Mineral. Petrol.* **76**, 99-120.

RAPOPORT, P.A. & BURNHAM, C.W. (1973): Ferrobustamite: the crystal structures of two Ca,Fe bustamite-type pyroxenoids. *Z. Kristallogr.* **138**, 419-438.

REVERDATTO, V.V., PERTSEV, N.N. & KOROLYUK, V.N. (1979): $PCO_2$ – T evolution of zoning in melilite during the regressive stage of contact metamorphism in carbonate-bearing rocks. *Contrib. Mineral. Petrol.* **70**, 203-208.

RUSSO-SANDULESCU, D. & BERZA, T. (1979): Banatites from the western part of the Southern Carpathians (Banat). *Rev. Roumaine Géol., Géophys. et Géogr., Géol.* **23**(2), 143-157.

_____, _____, BRATOSIN, I. & IANC, R. (1976): Petrological study of the Bocsa banatitic massif (Banat). *D.S. ale Sedintelor* **64**, 105-172.

RUTSTEIN, M.S. (1971): Re-examination of the wollastonite–hedenbergite ($CaSiO_3$–$CaFeSi_2O_6$) equilibria. *Am. Mineral.* **56**, 2040-2052.

SABINE, P.A. (1975): Metamorphic processes at high temperature and low pressure: the petrogenesis of the metasomatized and assimilated rocks of Carneal, Co. Antrim. *Phil. Trans. R. Soc. London* **A 280**, 225-269.

SACK, R.O. & GHIORSO, M.S. (1994a): Thermodynamics of multicomponent pyroxenes. I. Formulation of a general model. *Contrib. Mineral. Petrol.* **116**, 277-286.

_____ & _____ (1994b): Thermodynamics of multicomponent pyroxenes. III. Calibration of $Fe^{2+}(Mg)_{-1}$, $TiAl_2(MgSi_2)_{-1}$, $TiFe^{3+}{}_2(MgSi_2)_{-1}$, $AlFe^{3+}(MgSi)_{-1}$, $NaAl(CaMg)_{-1}$, $Al_2(MgSi)_{-1}$ and $Ca(Mg)_{-1}$ exchange reactions between pyroxenes and silicate melts. *Contrib. Mineral. Petrol.* **118**, 271-296.

SCACCHI, E. (1888): *Rendiconti Accademie Napoli*

SHEDLOCK, R.J. & ESSENE, E.J. (1979): Mineralogy and petrology of a tactite near Helena, Montana. *J. Petrol.* **20**, 71-97.

SHIMAZAKI, H. & YAMANAKA, T. (1973): Iron-wollastonite from skarns and its stability relations in the $CaSiO_3$–$CaFeSi_2O_6$ join. *Geochem. J.* **7**, 67-79.

ŞTEFAN, A., ISTRATE, G. & MEDESAN, A. (1978): Gehlenite in calc-skarns from Magureaua Vaţei – Cerboaia (Apuseni Mountains – Romania). *Rev. Roumaine Géol., Géophys. et Géogr., Géol.* **22**, 155-160.

TILLEY, C.E. (1938): Aluminous pyroxenes in metamorphosed limestones. *Geol. Mag.* **75**, 81-86.

_____ (1948): On iron-wollastonites in contact skarns: an example from Skye. *Am. Mineral.* **33**, 736-738.

_____ & HARWOOD, H.F. (1931): The dolerite–chalk contact of Scawt Hill, Co. Antrim. The production of basic alkali-rocks by assimilation of limestone by basaltic magma. *Mineral. Mag.* **22**, 439-468.

VAREKAMP, J.C. (1983): The significance of mafic nodules in the ultra-potassic rocks from central Italy – discussion. *J. Volcanol. Geotherm. Res.* **16**, 161-165.

WALDBAUM, D.R. (1973): The configurational entropies of $Ca_2MgSi_2O_7$–$Ca_2SiAl_2O_7$ melilites and related minerals. *Contrib. Mineral. Petrol.* **39**, 33-54.

WIECHMANN, M.J. (1995): *Contact Metamorphism and Skarn Formation at Crestmore, California.* Ph.D. thesis, Johns Hopkins University, Baltimore, Maryland.

WOOD, B.J. (1979): Activity–composition relationships in $Ca(Fe,Mg)Si_2O_6$–$CaAl_2SiO_6$ clinopyroxene solid solutions. *Am. J. Sci.* **279**, 854-875.

YAGI, K. & ONUMA, K. (1967): The join $CaMgSi_2O_6$–$CaTiAl_2O_6$ and its bearing on the titanaugites. *J. Fac. Sci. Hokkaido Univ., Ser.* 4, **13**, 463-483.

YANG, H.L. (1975): Al- and Ti-rich clinopyroxene in the system $CaMgSi_2O_6$–$CaAl_2SiO_6$–$CaTiAl_2O_6$. *Proc. Geol. Soc. China* **18**, 48-58.

*Received September 21, 2003, revised manuscipt accepted January 27, 2005.*